Akt-mediated phosphorylation of MICU1 regulates mitochondrial Ca²⁺ levels and tumor growth

Saverio Marchi[1],[*] (iD), Mariangela Corricelli[1], Alessio Branchini[2] (iD), Veronica Angela Maria Vitto[1], Sonia Missiroli[1], Giampaolo Morciano[1,3], Mariasole Perrone[1], Mattia Ferrarese[2], Carlotta Giorgi[1], Mirko Pinotti[2], Lorenzo Galluzzi[4,5] (iD), Guido Kroemer[5,6,7,8,9,10,11,12] (iD) & Paolo Pinton[1,3,**] (iD)

Abstract

Although mitochondria play a multifunctional role in cancer progression and Ca²⁺ signaling is remodeled in a wide variety of tumors, the underlying mechanisms that link mitochondrial Ca²⁺ homeostasis with malignant tumor formation and growth remain elusive. Here, we show that phosphorylation at the N-terminal region of the mitochondrial calcium uniporter (MCU) regulatory subunit MICU1 leads to a notable increase in the basal mitochondrial Ca²⁺ levels. A pool of active Akt in the mitochondria is responsible for MICU1 phosphorylation, and mitochondrion-targeted Akt strongly regulates the mitochondrial Ca²⁺ content. The Akt-mediated phosphorylation impairs MICU1 processing and stability, culminating in reactive oxygen species (ROS) production and tumor progression. Thus, our data reveal the crucial role of the Akt-MICU1 axis in cancer and underscore the strategic importance of the association between aberrant mitochondrial Ca²⁺ levels and tumor development.

Introduction

Mitochondrial Ca²⁺ accumulation controls cellular energetics and cell metabolism by favoring ATP production, and mitochondrial Ca²⁺ also operates as a key regulator of cell fate (Giorgi et al, 2018). Multiple pathological contexts, including tumor formation and development, are strictly linked to mitochondrial deregulation, and a hallmark feature of cancer cells is the re-programming of their mitochondrial metabolism (Hanahan & Weinberg, 2011; Boroughs & DeBerardinis, 2015). The connection between mitochondrial dysfunction and cancer is not only limited to the metabolic transformation of cancer cells but also triggers tumor-promoting epigenetic changes (Gottlieb & Tomlinson, 2005; Gaude & Frezza, 2014). Therefore, it is not surprising that several oncogenes and tumor suppressors exert their activities by regulating mitochondrial function (Galluzzi et al, 2012; Frezza, 2014) and that many of them act on key Ca²⁺-transport molecules to provoke deep mitochondrial Ca²⁺ homeostasis remodeling and promote certain malignant phenotypes (Prevarskaya et al, 2011; Danese et al, 2017).

The mitochondrial calcium uniporter (MCU), which is the channel that is responsible for Ca²⁺ accumulation inside the mitochondrial matrix, has been recently characterized at the molecular level (Baughman et al, 2011; De Stefani et al, 2011). Moreover, a series of proteins that contribute to the formation of the so-called MCU complex have also been identified (Giorgi et al, 2018). Such proteins include the dominant-negative form MCUb (Raffaello et al, 2013), the essential regulator EMRE (Sancak et al, 2013), and others that regulate MCU channel activity, such as MICU1 (Perocchi et al, 2010) and its paralog MICU2 (Plovanich et al, 2013). Among the different components of the mitochondrial Ca²⁺ uptake machinery, MICU1 functions have been the subject of extensive studies that revealed that MICU1 acts as a gatekeeper for the MCU complex, setting the threshold for mitochondrial Ca²⁺ uptake (Mallilankaraman et al, 2012; Csordas et al, 2013). Although genetic MICU1 ablations in both cells and tissues and loss-of-function

1   Laboratory for Technologies of Advanced Therapies (LTTA), Department of Morphology, Surgery and Experimental Medicine, Section of Pathology, Oncology and Experimental Biology, University of Ferrara, Ferrara, Italy
2   Department of Life Sciences and Biotechnology, University of Ferrara, Ferrara, Italy
3   Maria Cecilia Hospital, GVM Care & Research, Cotignola, Italy
4   Department of Radiation Oncology, Weill Cornell Medical College, New York, NY, USA
5   Université Paris Descartes, Sorbonne Paris Cité, Paris, France
6   Equipe 11 Labellisée Ligue Nationale Contre le cancer, Centre de Recherche des Cordeliers, Paris, France
7   Institut National de la Santé et de la Recherche Médicale, U1138, Paris, France
8   Université Pierre et Marie Curie, Paris, France
9   Metabolomics and Cell Biology Platforms, Gustave Roussy Cancer Campus, Villejuif, France
10 Center of Clinical Investigations in Biotherapies of Cancer (CICBT), Villejuif, France
11 Pôle de Biologie, Hôpital Européen Georges Pompidou, AP-HP, Paris, France
12 Department of Women's and Children's Health, Karolinska University Hospital, Stockholm, Sweden
    *Corresponding author. Tel: +39 0532 455858; E-mail: saverio.marchi@unife.it
    **Corresponding author. Tel: +39 0532 455802; E-mail: paolo.pinton@unife.it

mutations in the *MICU1* gene have been associated with different pathological scenarios (Logan *et al*, 2014; Antony *et al*, 2016), little is known about the role of MICU1-related mitochondrial Ca^{2+} homeostasis in tumor progression. Recent evidence indicates that both prostate and colon cancer cells overexpress cancer-related microRNAs that target the channel pore-forming subunit MCU, thus conferring resistance to apoptotic stimuli (Marchi, *et al*, 2013). Moreover, *MCU* expression correlates with breast cancer progression, and the deletion of *MCU* reduces tumor growth and metastasis formation (Tosatto *et al*, 2016). No correlation has been observed between the expression of MCU regulators and tumor size, raising the possibility that instead of quantitative changes, qualitative alterations determined by post-translational modifications could account for the altered MCU function in oncogenesis (Tosatto *et al*, 2016).

Here, we show that phosphorylation at the N-terminal domain of the MICU1 protein robustly alters the basal mitochondrial Ca^{2+} content under resting conditions. The target amino acid residue is contained in an Akt consensus phosphorylation motif, and MICU1 is readily phosphorylated upon Akt activation inside the mitochondrial compartment. Akt-mediated phosphorylation affects MICU1 proteolytic maturation and stability, thereby explaining the altered mitochondrial Ca^{2+} homeostasis. Importantly, the expression of a nonphosphorylatable MICU1 mutant significantly reduces the *in vivo* growth rate of tumors, even in the presence of activated Akt, suggesting a key role for the mitochondrial Akt-MICU1 axis in cancer progression.

Results

N-terminal MICU1 phosphorylation increases the basal mitochondrial Ca^{2+} levels

We investigated the potentially phosphorylated residues in the MICU1 sequence. Using the Scansite 3 software program (http://scansite3.mit.edu), we searched for motifs within the wild-type (WT) MICU1 protein (NM_144822) that are likely to be phosphorylated by specific protein kinases. The following three candidates were identified: Ser124, Ser195, and Thr256 (Fig 1A). Among them, Ser124 displayed the highest value of surface accessibility, as well as a high phosphorylation prediction score (Fig 1A). Ser124 is localized in the N-terminal region of MICU1, which has been proposed to extend into the intermembrane space (Csordas *et al*, 2013). As a result, we generated two MICU1 mutants, a nonphosphorylatable S124A and a phosphomimetic S124D MICU1 mutant. When transfected into cells, both mutated MICU1 proteins localized correctly to mitochondria (Fig 1B). It is now widely accepted that MICU1 functions as a gatekeeper of the MCU channel, meaning that loss of MICU1 facilitates Ca^{2+} accumulation inside the mitochondrial matrix even at low cytosolic Ca^{2+} levels (Mallilankaraman *et al*, 2012). Thus, we transfected the mitochondrial matrix-targeted Ca^{2+} biosensor GCaMP6m into cells expressing the MICU1 WT or SD and SA mutants. Due to its characteristics as a ratiometric sensor, GCaMP6m is reputed to quantitatively measure even small differences in the resting mitochondrial Ca^{2+} concentration ([Ca^{2+}]m) (Hill *et al*, 2014). We expressed WT or mutant forms of MICU1 in cells from which endogenous MICU1 was constitutively depleted using a short hairpin RNA (shRNA) (Fig EV1A). As expected, the

resting mitochondrial Ca^{2+} levels were largely increased when *MICU1* was stably downregulated, and the expression of both the WT MICU1 and SA mutant reduced the baseline [Ca^{2+}]m levels in Sh*MICU1* cells. In contrast, the MICU1 SD variant failed to restore [Ca^{2+}]m in Sh*MICU1* cells (Fig 1C and D). To verify the role of Ser124 phosphorylation in the regulation of MICU1 functionality, we analyzed the mitochondrial Ca^{2+} uptake following treatment with the sarcoplasmic/endoplasmic reticulum Ca^{2+} ATPase (SERCA) inhibitor 2,5-di-tert-butylhydroquinone (TBHQ), which induces slow and weak ER Ca^{2+} depletion (Waldeck-Weiermair *et al*, 2015). The co-transfection of the MICU1 WT, SD mutant, or SA mutant with an aequorin-based mitochondrial Ca^{2+} probe revealed that only mock and MICU1 SD-expressing cells were able to accumulate [Ca^{2+}]m under these conditions, whereas the MICU1 WT and SA mutant failed to do so (Fig 1E and F). We obtained similar results when TBHQ was replaced with another SERCA antagonist, cyclopiazonic acid (CPA) (Fig 1G and H). The higher Ca^{2+} affinity of the MICU1 SD mutant-expressing mitochondria was also investigated in permeabilized cells. After permeabilization in an EGTA-containing Ca^{2+}-free buffer (IB/EGTA) that mimics the physiological ion milieu, Ca^{2+} uptake was generated by switching the perfusion buffer to IB, containing EGTA-buffered Ca^{2+}. Using different [Ca^{2+}]s (500, 800 nM, and 1.5 μM), the rates of mitochondrial Ca^{2+} uptake were substantially increased in both *MICU1*-depleted and SD-expressing cells (Fig EV1B). Interestingly, MICU1 SA mutant slightly lowered the Ca^{2+} threshold for channel activation, showing reduced Ca^{2+} uptake rate compared to MICU1 WT (Fig EV1B). Overall, these data suggest that upon phosphorylation of serine 124, MICU1 loses its inhibitory function on the MCU complex.

To further demonstrate this concept, we analyzed the basal mitochondrial Ca^{2+} levels in intact HeLa cells. Overexpression of the MICU1 WT or MICU1 SA mutant caused no significant changes in the basal mitochondrial Ca^{2+} levels compared with those found in untransfected control cells. However, the basal mitochondrial Ca^{2+} content in the MICU1 SD-overexpressing cells was significantly increased compared to that in the MICU1 WT- and MICU1 SA-expressing cells (Appendix Fig S1A). These data are independent from changes in the mitochondrial membrane potential (Appendix Fig S1B) and were confirmed using both TBHQ and CPA inhibitors (Appendix Fig S1C–F).

Because the protein levels of MICU1 and MCU and their stoichiometry are crucial aspects in regulating [Ca^{2+}]m (Paillard *et al*, 2017), we reconstituted the MICU1 WT and mutants in a MICU1-null background, generated using a CRISPR/CAS9-mediated approach (Fig 1I). Using the mito-GCaMP6m indicator, we observed higher Ca^{2+} levels only in MICU1-null and MICU1 SD-expressing cells (Fig 1J). Similar findings were obtained with an aequorin-based approach upon stimulation with either TBHQ or CPA (Fig 1K–N).

Therefore, the results achieved in three different cell lines and using three different techniques to measure [Ca^{2+}]m, namely (i) in untreated intact cells, (ii) upon treatment of intact cells with SERCA antagonists, and (iii) upon Ca^{2+} addition to permeabilized cells, indicate that phosphorylation of MICU1 at position 124 limits its negative effect on MCU and thus induces Ca^{2+} accumulation inside the mitochondrial matrix. Based on these results, we became interested in identifying the kinase responsible for MICU1 phosphorylation.
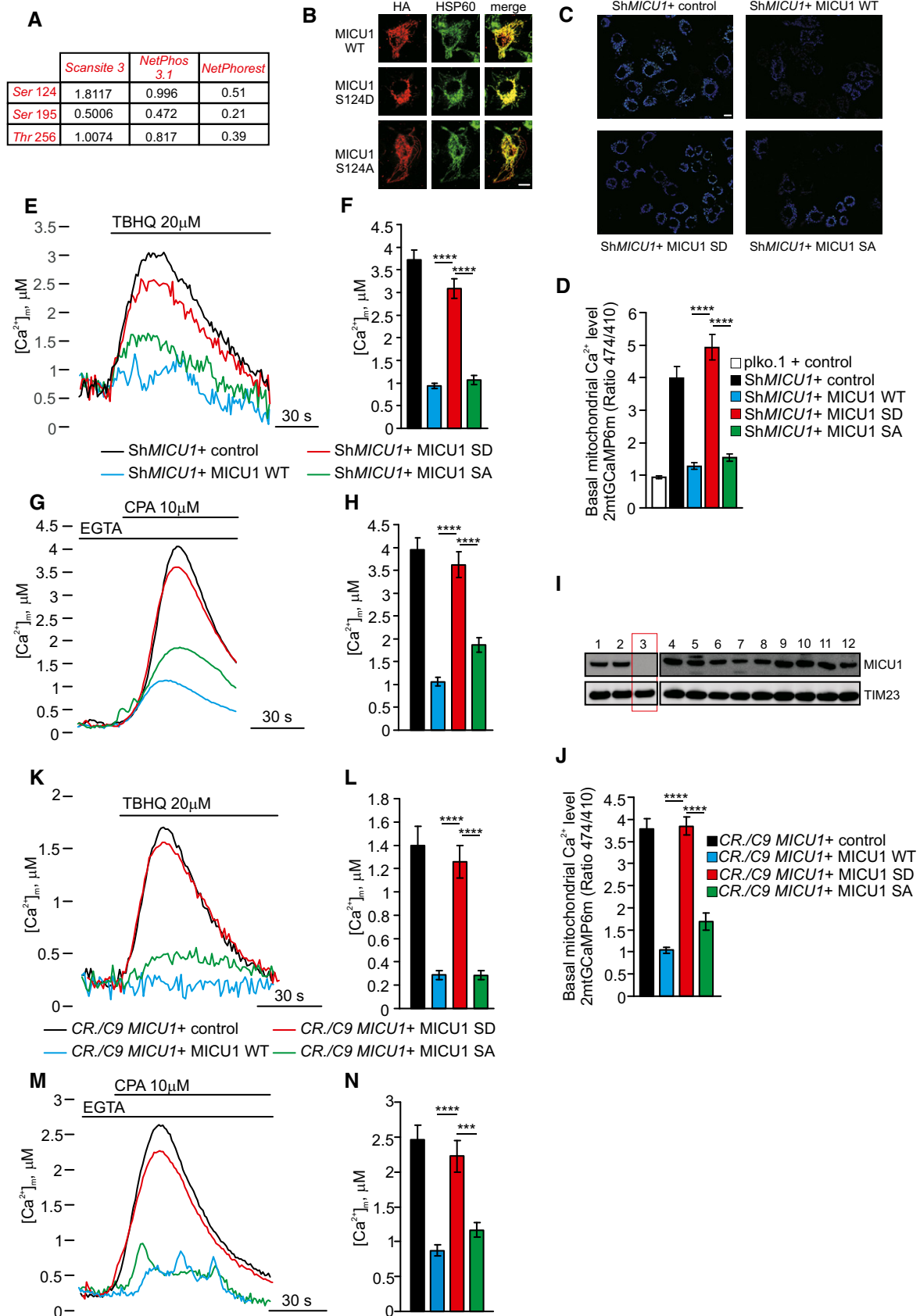
Figure 1.

MICU1 phosphorylation is mediated by mitochondrial Akt

The MICU1 sequence surrounding Ser124 matches the Akt consensus phosphorylation motif, R-X-R-X-X-S/T (Manning & Cantley, 2007), which is highly conserved among different species (Fig 2A). We observed that upon treatment with rapamycin, which is a known activator of Akt, a significant number of cells displayed an obvious mitochondrial localization of activated (Ser473 phosphorylated) Akt (Fig 2B and C and Appendix Fig S2A). Subcellular fractionation followed by immunoblot analyses suggested that the treatment of HEK293T cells with rapamycin resulted in an increased Akt activation/phosphorylation to mitochondria (Appendix Fig S2B). This effect was observed not only in the crude mitochondrial fractions (Appendix Fig S2B), but also highly purified mitochondria without any detectable plasma membrane contamination (Fig 2D). Consistent with these results, pure mitochondria extracted from mouse livers after *in vivo* exposure to rapamycin also contained higher levels of Akt with phosphorylated Ser473 (Fig 2E). Having established the existence of a rapamycin-induced pool of active Akt in mitochondria, we sought to determine its submitochondrial localization. Proteinase K (PK) digestion of purified mitochondria that were subjected to selective outer membrane permeabilization by osmotic swelling (i.e., via the removal of sucrose) or complete lysis with Triton X-100 revealed that MICU1 behaved similarly to the inner mitochondrial membrane (IMM)–intermembrane space (IMS) protein TIM23 (both of which became susceptible to proteolysis after outer membrane permeabilization), in contrast to the matrix proteins HSP60 and MCU, which only became digested when the detergent was added (Fig 2F). This finding indicates that MICU1 is located at the outer surface of the IMM, as previously suggested (Csordas *et al*, 2013; Tsai *et al*, 2016). Importantly, in response to rapamycin, active Akt located predominantly at the IMS and, to a lesser extent, in the matrix compartment (Fig 2F). Alkaline carbonate extraction of isolated HEK293T cell mitochondria revealed that active Akt is loosely attached to the IMM, sharing this characteristic with cytochrome *c* (Fig 2G). Taken together, these results demonstrate that active Akt

localizes in the mitochondria in a membrane-unbound state and accumulates in the same submitochondrial compartment as MICU1.

We then immunoprecipitated WT MICU1-GFP and analyzed its phosphorylation status following rapamycin treatment with an antibody that recognizes the Akt consensus phosphorylation protein sequence, R-X-R-X-X-S/T (anti-PAS, phospho-Akt substrate antibody). The MICU1-GFP immune complexes reacted with the PAS antibody preferentially in the rapamycin-treated cells, and triciribine, which is an allosteric inhibitor of Akt activation (Yang *et al*, 2004; Littlepage *et al*, 2012), counteracted this reaction (Fig 2H). Accordingly, the immune complexes precipitated with the anti-PAS antibody upon rapamycin stimulation of Akt (Fig EV1C). Moreover, rapamycin increased the reactivity of the MICU1-GFP immune complexes with an antibody that detects proteins with phosphorylated serine residues (anti-p-Ser) (Fig EV1D), suggesting that the Akt-mediated phosphorylation of MICU1 occurs at a specific serine residue. To verify that Ser124 is the Akt target site on MICU1, we immunoprecipitated the GFP-tagged MICU1 WT and MICU1-S124A mutant and then analyzed the MICU1 phosphorylation status using the PAS antibody. As shown in Fig 2I, rapamycin induced phosphorylation of the WT MICU1 but failed to stimulate the phosphorylation of the defective mutant S124A. Notably, quantitation of the basal $[Ca^{2+}]$m content using the mito-GCaMP6m probe revealed that rapamycin increased $[Ca^{2+}]$m in the WT MICU1-transfected cells, but the corresponding increase in the MICU1 SA mutant-transfected cells was decreased (Fig EV1E). The knockdown of Akt in HeLa cells (Fig EV1F) significantly attenuated the rapamycin-induced $[Ca^{2+}]$m elevation (Fig EV1G), further confirming that Akt is critical for this pathway. Moreover, rapamycin did not induce Ca^{2+} release from the stores (Fig EV1H) and consequent cytosolic Ca^{2+} elevation (Fig EV1I), suggesting that the rapamycin-mediated $[Ca^{2+}]$m rise is related to Akt mitochondrial activity.

Overall, these findings indicate that rapamycin promotes the translocation of activated Akt to mitochondria, thereby inducing Akt-mediated N-terminal MICU1 phosphorylation and a consequent increase in $[Ca^{2+}]$m.
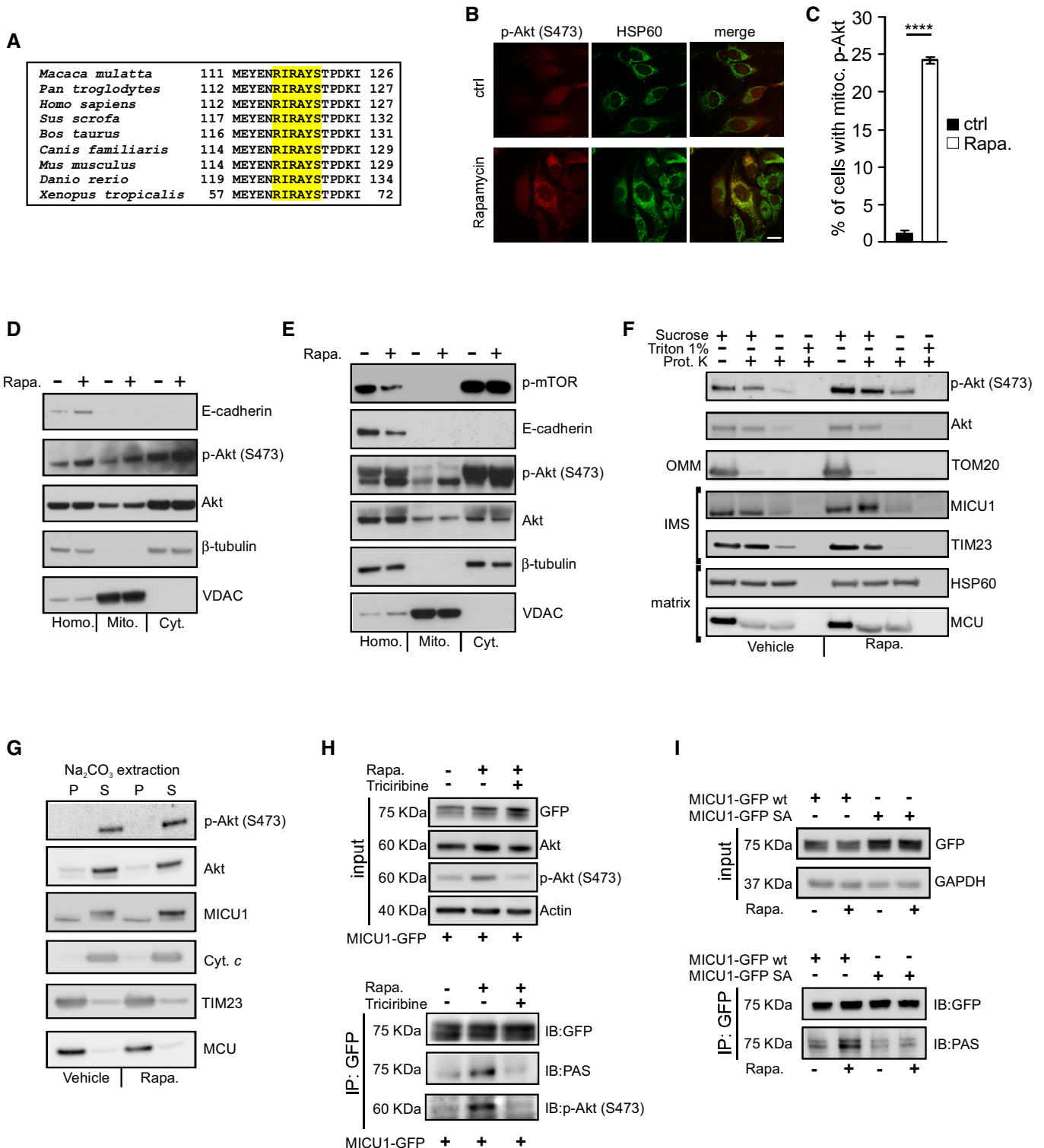
Figure 2.

Mitochondrion-targeted Akt increases the basal $[Ca^{2+}]m$ content in an MICU1-dependent manner

To further investigate the role of Akt in the regulation of mitochondrial Ca^{2+} dynamics, we used a constitutively active Akt form (Akt D/D), which has previously been reported to localize inside the mitochondrial compartment (Barksdale & Bijur, 2009). Transfection-mediated Akt D/D overexpression caused a significant pool of the Akt construct to be located in mitochondria (Fig 3A), with a concomitant increase in $[Ca^{2+}]m$ under resting conditions (Fig 3B).

◄

Figure 2. Mitochondrial Akt phosphorylates MICU1 at the Ser124 position.

A   Sequence alignment of the MICU1 protein from nine vertebrate species. The Akt consensus phosphorylation motif, R-X-R-X-X-S/T, is marked in yellow.

B   HeLa cells treated with vehicle or 1 μM rapamycin for 4 h were stained for phosphorylated (S473) Akt (p-Akt) or HSP60 (mitochondrial marker). Merged images are indicated (merge). Scale bar 10 μm.

C   Analysis of the number of cells, expressed as a percentage, showing obvious mitochondrial staining of activated (S473 phosphorylated) Akt (p-Akt) (n = 3 independent experiments; 350-355 cells). Means $\pm$ SEM. ****P < 0.0001 (Student's t-test).

D   HEK293T cells treated with vehicle or 1 μM rapamycin (Rapa.) for 4 h were fractionated into cytosol (Cyt.) or mitochondrial (Mito.) extracts and analyzed by Western blotting. E-cadherin: plasma membrane marker; β-tubulin: cytosolic marker; VDAC: mitochondrial marker; Homo: cell homogenate.

E   Mouse livers treated with vehicle or 1 μM rapamycin (Rapa.) for 16 h by an intraperitoneal injection were fractionated into cytosol (Cyt.) or mitochondrial (Mito.) extracts and analyzed by Western blotting. Phosphorylated (S2468) mTOR (p-mTOR) was used to assess the rapamycin activity. E-cadherin: plasma membrane marker; β-tubulin: cytosolic marker; VDAC: mitochondrial marker; Homo: cell homogenate.

F   Mitochondria isolated from HEK293T cells were subjected to the indicated treatments and analyzed by Western blotting against Akt, phosphorylated (S473) Akt (p-Akt), and mitochondrial proteins with known localizations. Osmotic swelling through the removal of sucrose from the buffer was used to induce OMM rupture. OMM: outer mitochondrial membrane; IMS: intermembrane space.

G   Western blot analysis of the supernatant (S) and insoluble pellet (P) fractions of vehicle- or rapamycin (Rapa., 1 μM for 4 h)-treated HEK293T cell mitochondria following carbonate extraction at pH 11.5. Akt, phosphorylated (S473) Akt (p-Akt), MICU1, the established integral membrane proteins TIM23 and MCU, and the soluble protein cytochrome c (Cyt. c) was analyzed.

H   HEK293T cells were transfected with the GFP-tagged wild-type (WT) MICU1 and then treated with 1 μM rapamycin (Rapa.) alone for 4 h or in combination with the Akt inhibitor triciribine (10 μM). GFP-MICU1 immunocomplexes were precipitated with a GFP antibody and analyzed with PAS (phospho-Akt substrate) and phosphorylated (S473) Akt (p-Akt) antibodies by Western blotting.

I   HEK293T cells were transfected with either the GFP-tagged wild-type (WT) MICU1 or MICU1 S124A-GFP mutant. MICU1-GFP immunocomplexes were precipitated with a GFP antibody and analyzed with PAS (phospho-Akt substrate) antibody by Western blotting.

Source data are available online for this figure.

To investigate whether the Akt D/D mutant might specifically regulate mitochondrial Ca^{2+} homeostasis, we measured the Ca^{2+} concentrations in different intracellular compartments, including the ER and cytosol, using the aequorin technique. Control cells and Akt D/D-expressing cells revealed similar ER Ca^{2+} kinetics (Fig EV2A and B) and cytosolic Ca^{2+} levels (Fig EV2C and D), which is in line with the notion that the alteration in $[Ca^{2+}]m$ induced by Akt D/D expression is indeed due to local effects. Importantly, a membrane-targeted active form of Akt kinase (m/p-Akt), which has been described to inhibit ER Ca^{2+} release through IP3R binding and phosphorylation (Szado *et al*, 2008; Marchi *et al*, 2012), interacted with type 3 IP3R, whereas Akt D/D failed to do so (Fig EV2E). These data are consistent with prior reports indicating that the Akt D/D construct, which is active without membrane targeting (Dufner *et al*, 1999), does not act at the level of the ER and is unable to phosphorylate IP3R (Khan *et al*, 2006). Moreover, the expression of Akt D/D in the MICU1-silenced cells did not further increase the basal $[Ca^{2+}]m$ levels (Fig EV2F), suggesting that its effects are largely dependent on MICU1.

To further explore the Ca^{2+}-related activities of Akt inside mitochondria, we generated a HA-tagged active Akt chimera targeted to the mitochondrial IMS (mt-Akt D/D) (Fig 3C). The construct correctly localized to this mitochondrial compartment (Fig 3C) and promoted MICU1 phosphorylation (Fig 3D and E). Measurements of basal $[Ca^{2+}]m$ revealed that mt-Akt D/D overexpression evoked higher Ca^{2+} levels in unstimulated cells (Fig 3F). Consistently, this increase in $[Ca^{2+}]m$ by mt-Akt D/D did not occur in MICU1-depleted cells (Fig EV2G). Therefore, mt-Akt D/D is sufficient to elevate basal $[Ca^{2+}]m$ even in the absence of rapamycin through an effect that requires MICU1.

To confirm that serine 124 in the MICU1 sequence is the target residue of the mitochondrial Akt kinase activity, we analyzed the $[Ca^{2+}]m$ levels upon expression of the mt-Akt D/D chimera together with different MICU1 mutants. mt-Akt D/D was capable of elevating the resting $[Ca^{2+}]m$ levels in the presence of the WT MICU1 form but not with the nonphosphorylatable MICU1 SA mutant (Fig 3G). Moreover, in MICU1 SD-expressing cells, mt-Akt D/D had no

additional effects on $[Ca^{2+}]m$ (Appendix Fig S3A). Second, in a permeabilized cell-based experiment, the reconstitution of MICU1-silenced cells with the WT MICU1, but not with the MICU1 SA mutant, yielded a higher Ca^{2+}-stimulated mitochondrial increase in $[Ca^{2+}]m$ in the presence of mt-Akt D/D (Fig 3H and I). The role of mitochondrial Akt in the regulation of basal Ca^{2+} levels is strictly dependent on its activation, since a mitochondrial-targeted Akt WT construct (mt-Akt WT) (Appendix Fig S3B) induced a marginal increase in $[Ca^{2+}]m$ (Appendix Fig S3C).

Taken together, these data support a model in which active Akt that is located at the mitochondrial IMS promotes higher $[Ca^{2+}]m$ through the inhibitory phosphorylation of MICU1.

Phosphorylation affects MICU1 processing and destabilizes the MICU1-MICU2 heterodimer

We focused on the molecular alterations induced by Akt-mediated MICU1 phosphorylation. When we reconstituted the essential uniporter complex by co-transfecting MCU and EMRE with different MICU1 forms, we observed a notable reduction in the mature MICU1 levels only when the MICU1 SD mutant was present, which appeared to accumulate in an unprocessed form (Fig 4A and B). It has been proposed that MICU1 undergoes multiple cleavage steps to become completely mature (Petrungaro *et al*, 2015). We wanted to investigate whether phosphorylation could affect the correct processing of MICU1. We hypothesized that MICU1 could fall into the first class of IMS proteins, which are first cleaved by a matrix protease, integrated in the IMM and then subjected to a second cleavage event that ensures the release of the mature protein into the IMS (Herrmann & Hell, 2005). Thus, defects in the second stage of processing result in an accumulation of the intermediate form, which is locked into the IMM. Mature WT MICU1 and the SA mutant were recovered in the supernatant fraction following alkaline extraction, whereas SD accumulated in the intermediate form and was more tightly associated with membranes (Fig 4C). Consistently, larger forms of MICU1 SD were mainly recovered in the pellet fractions and were detected only in the supernatant fraction at pH
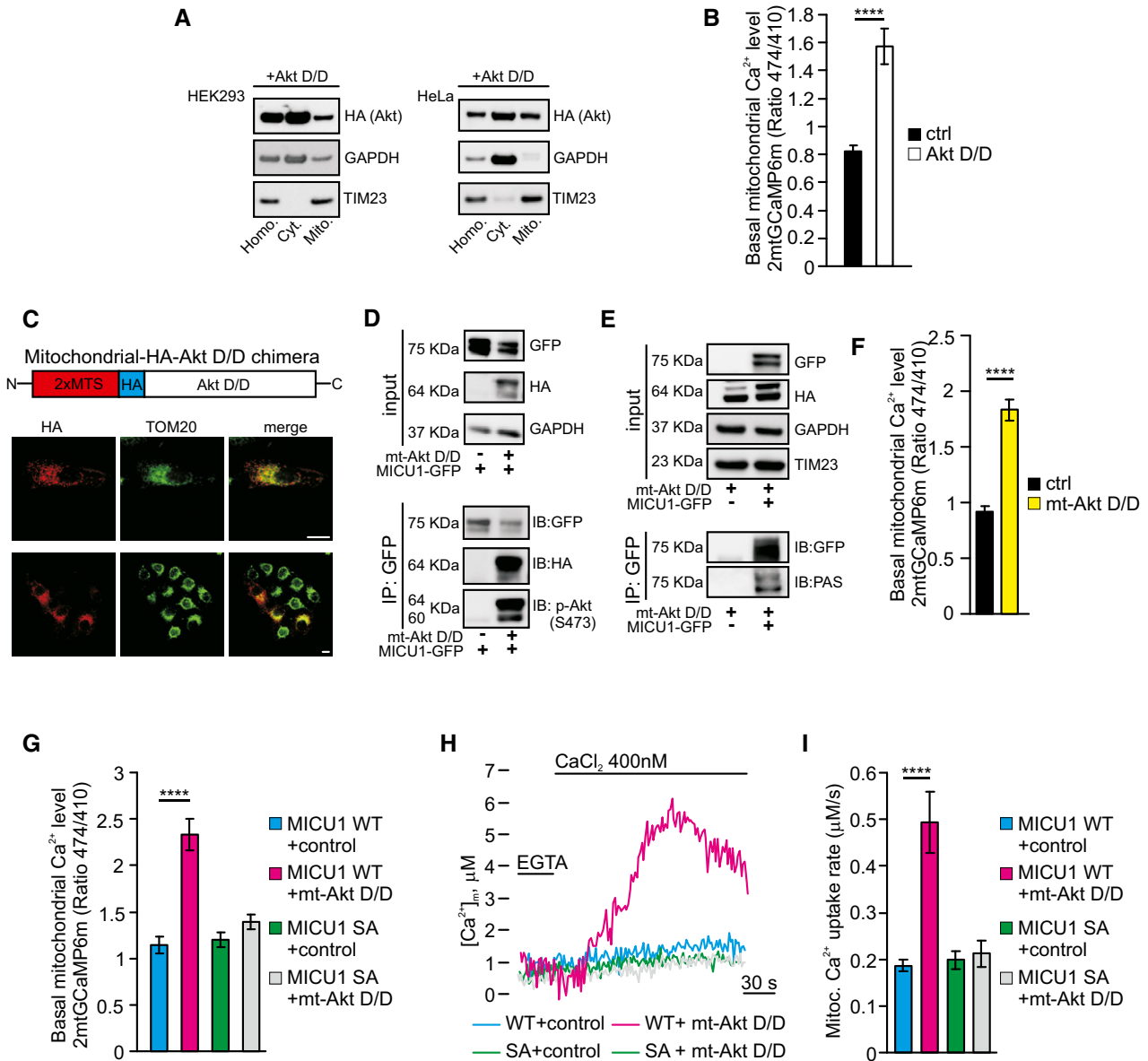
Figure 3. Mitochondrial Akt augments the basal Ca²⁺ levels in a MICU1-dependent manner.

A   Mitochondrial preparations of both HEK293T (left) and HeLa (right) cells transiently transfected with an HA-tagged constitutively active Akt T308D/S473D (Akt D/D) construct were analyzed by Western blotting. GAPDH: cytosolic marker; TIM23: mitochondrial marker.

B   Resting mitochondrial calcium levels in the control (ctrl) and Akt D/D-expressing HeLa cells evaluated by ratiometric imaging of the mitochondrial-targeted GCaMP6m (n = 4 independent experiments; 44–49 cells).

C   Schematic model of the HA-tagged constitutively active Akt form targeted to the mitochondrial intermembrane space (mt-Akt D/D). Both the expression and the mitochondrial localization of the chimera were assessed by immunofluorescence. TOM20 was used as a mitochondrial marker. Merged images are indicated (merge). Scale bar 10 μm.

D   HEK293T cells were transfected with the indicated constructs. The GFP-tagged MICU1 was immunoprecipitated from the whole-cell lysate, and the precipitated proteins were immunoblotted with the HA and phosphorylated (S473) Akt (p-Akt) antibodies.

E   HEK293T cells were transfected with the indicated constructs. MICU1-GFP immunocomplexes were precipitated with a GFP antibody and analyzed with PAS (phospho-Akt substrate) antibody by Western blotting.

F   Resting mitochondrial calcium levels in control (ctrl) and mitochondrial-targeted Akt D/D (mt-Akt D/D)-expressing HeLa cells, evaluated through ratiometric imaging of the mitochondrial-targeted GCaMP6m (n = 4 independent experiments; 43–47 cells).

G   Resting mitochondrial calcium levels in ShRNA *MICU1* HeLa stable cells transfected with the indicated constructs and evaluated through ratiometric imaging of the mitochondrial-targeted GCaMP6m (n = 3 independent experiments; 38–50 cells).

H, I   Representative kinetics (H) and analysis (I) of aequorin-based [Ca²⁺]m measurements in permeabilized ShRNA *MICU1* HeLa stable cells transfected with the indicated constructs and challenged with 400 nM buffered [Ca²⁺] (n = 3 independent experiments).

Data information: (B, F) Means ± SEM. ****P < 0.0001 (Student's *t*-test); (G, I) Means ± SEM. ****P < 0.0001 (one-way ANOVA).
Source data are available online for this figure.
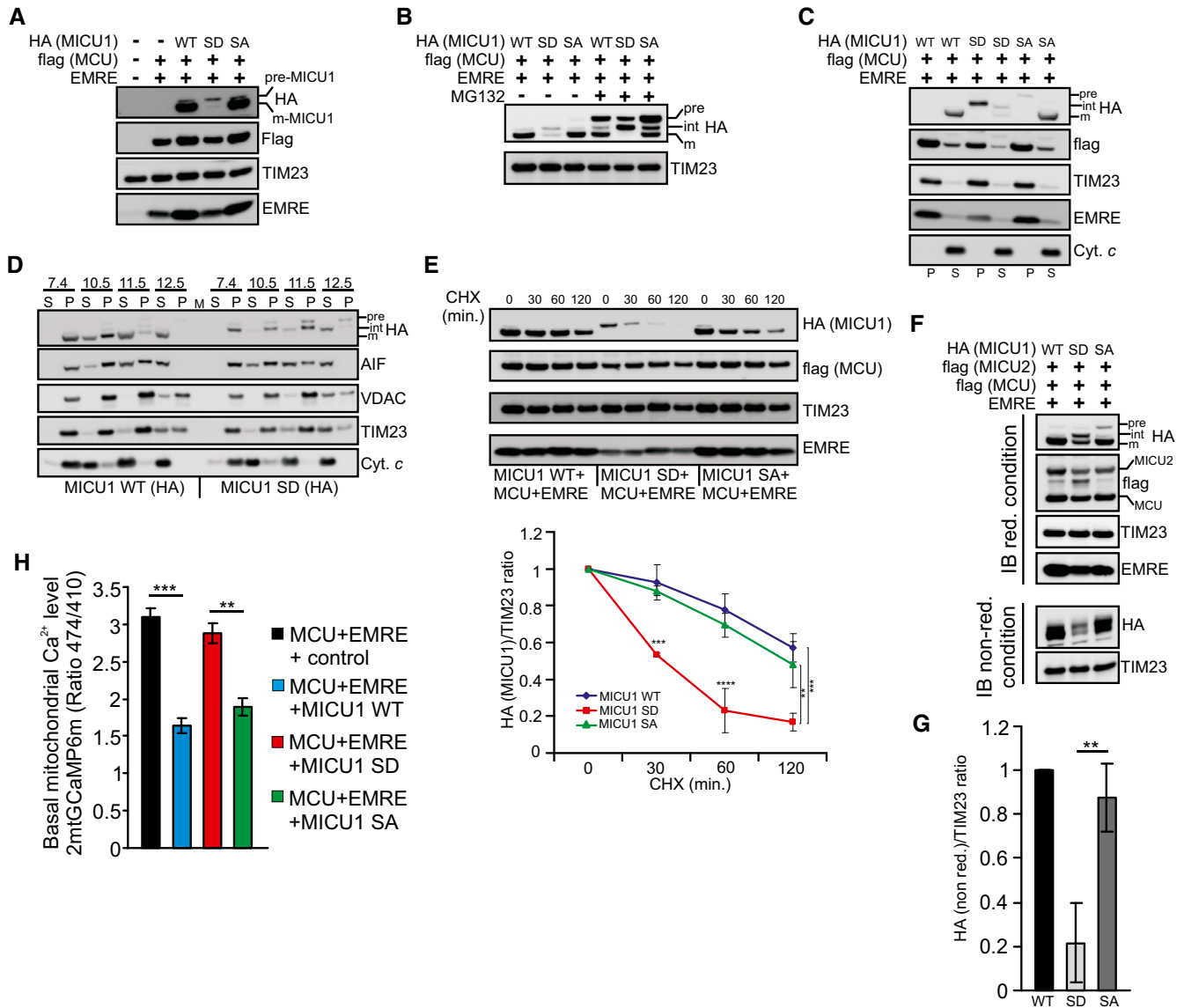
Figure 4. Akt-mediated phosphorylation of MICU1 affects protein maturation and stability.

A   Western blot analysis of ShRNA *MICU1* HeLa stable cells transfected with the indicated constructs. pre-MICU1: precursor form of MICU1; m-MICU1: mature form of MICU1.

B   Western blot analysis of ShRNA *MICU1* HeLa stable cells transfected with the indicated constructs. Where indicated, the cells were treated with 5 μM MG132 for 4 h. pre: precursor; int: intermediate; m: mature form.

C   Western blot analysis of the supernatant (S) and insoluble pellet (P) fractions of ShRNA *MICU1* HeLa cell mitochondria transfected with the indicated constructs, following carbonate extraction at pH 10. The established integral membrane protein TIM23 and the soluble protein cytochrome *c* (Cyt. *c*) were analyzed as markers. The cells were treated with 5 μM MG132 for 4 h before fractionation.

D   Western blot analysis of the supernatant (S) and insoluble pellet (P) fractions of ShRNA *MICU1* HeLa cell mitochondria transfected with MICU1 WT-HA or MICU1 SD-HA, together with MCU-flag and EMRE constructs, following carbonate extraction at pH 7.4, pH 10.5, pH 11.5, or pH 12.5. The cells were treated with 5 μM MG132 for 4 h before fractionation.

E   ShRNA *MICU1* HeLa stable cells were transfected with the indicated constructs. Cells were incubated with 50 μg/ml cycloheximide (CHX) for the indicated times, collected, and subjected to Western blotting analysis as indicated. In the graph, the amount of HA (MICU1), both WT and mutants, is represented relative to the amount at time 0 (*n* = 3 independent experiments).

F   ShRNA *MICU1* HeLa stable cells were transfected with the indicated constructs. Cells were harvested, and total protein was extracted and subjected to Western blotting analysis with the indicated antibodies. Immunoblotting was performed under reducing (with the presence of DTT) or non-reducing (non-red) conditions (without DTT). Cells were treated with 5 μM MG132 for 4 h before lysis.

G   Quantification of HA levels in non-reducing condition showed in (E) (*n* = 3 independent experiments).

H   Resting mitochondrial calcium levels, evaluated through ratiometric imaging of the mitochondrial-targeted GCaMP6m, in ShRNA *MICU1* HeLa stable clone cells transfected with the indicated constructs (*n* = 3 independent experiments; 46–54 cells).

Data information: (E, G) Means ± SD. **$P < 0.01$; ***$P < 0.001$; ****$P < 0.0001$ (one-way ANOVA); (H) Means ± SEM. **$P < 0.01$; ***$P < 0.001$ (one-way ANOVA). Source data are available online for this figure.

12.5 (Fig 4D). To test the function of Akt in this process, we performed immunoprecipitation experiments on sodium carbonate extracts from MICU1 WT-expressing cells, treated or not with rapamycin. We observed a strong PAS reactivity only in the rapamycin-treated pellet fraction (Fig EV3A), indicating a key role of Akt in the regulation of MICU1 processing and membrane association. Notably, the expression of active mitochondrial Akt chimera inhibited MICU1 maturation, which was only slightly affected by the mt-Akt WT form (Fig EV3B). Moreover, mt-Akt D/D induces accumulation of larger forms of MICU1 in the pellet fractions upon alkaline extraction of mitochondrial membranes, whereas MICU1 WT alone is easily released by sodium carbonate (Fig EV3C).

It has been proposed that partial proteolysis would be required to convert the unstable precursor intermediates into stable mature proteins (Vogtle *et al*, 2009, 2011). Therefore, we investigated whether the phosphorylation step in the MICU1 protein might impact MICU1 stability. When protein synthesis was inhibited with cycloheximide (CHX) to measure the half-life of MICU1, the MICU1 SD mutant degraded more rapidly than the WT protein and the SA mutant (Fig 4E). Moreover, co-expression of the MICU1 WT with the mitochondrial Akt construct reduced its half-life (Appendix Fig S4A), whereas MICU1 SA mutant maintains higher stability also in the presence of mito-Akt D/D (Fig EV3D).

It has previously been reported that MICU2 requires MICU1 for its stability but not *vice versa* (Plovanich *et al*, 2013). Therefore, we sought to determine whether the relative instability of phosphorylated MICU1 might entail a concomitant reduction in MICU2 stability. Consistent with the recent literature, we observed very low amounts of MICU2 in the *MICU1*-depleted cells (Fig EV3E). Importantly, the stable expression of the MICU1 SA mutant, but not that of the MICU1 SD mutant, in Sh*MICU1* cells restored the MICU2 levels (Fig EV3F). These findings were not affected by alterations in MICU1-2 binding because WT MICU1 and the two phosphomimetic and phosphorylation-resistant mutants similarly co-immunoprecipitated with flag-tagged MICU2 (Appendix Fig S4B). Immunoblot analysis in non-reducing conditions revealed that MICU1 SD expression strongly reduced the formation of the disulfide-linked MICU1-2 dimer (Fig 4F and G). These results were also observed in rapamycin-treated cells, and this effect was abolished by concomitant addition of the Akt inhibitor triciribine (Fig EV3G).

Finally, we analyzed the Ca^{2+} levels upon reconstitution of MICU1 plus the minimal uniporter components. The expression of MCU and EMRE in a MICU1-KD background increased the basal mitochondrial $[Ca^{2+}]$ content, which was significantly lowered by the MICU1 WT and SA mutant, but not by the SD construct (Fig 4H).

Altogether, we concluded that the Akt-mediated phosphorylation of MICU1 affects its maturation process, resulting in instability of MICU1 and the MICU1-2 dimer and defective mitochondrial Ca^{2+} regulation.

Inhibition of MICU1 maturation recapitulates all the effects observed upon MICU1 SD expression

To substantiate the crucial role of MICU1 processing in mitochondrial Ca^{2+} regulation, we planned to inhibit MICU1 maturation by preventing the second cleavage event, thereby inducing the accumulation of the intermediate form (Fig EV4A). We investigated the

processing peptidases mitochondrial inner membrane protease subunit 1 (IMMP1L) and IMMP2L, which have been indicated to promote protein maturation and activation by removing hydrophobic sorting signals from proteins that are sorted to the IMS, usually after these proteins have been first cleaved by matrix peptidases (Quiros *et al*, 2015). *IMMP1L*- and, to a lesser extent, *IMMP2L*-silencing (Appendix Fig S5A) inhibited MICU1 processing (Fig 5A and B), increasing the accumulation of the intermediate form and its association with membranes (Fig 5C and D). As previously observed for SD mutant expression, affecting MICU1 maturation promoted its degradation (Fig 5E and Appendix Fig S5B) and decreased the stability of the MICU1-2 dimer (Appendix Fig S5C). Finally, we measured the basal mitochondrial $[Ca^{2+}]$ upon *IMMP1L* depletion. Both aequorin-based (Fig 5F and G) and GCaMP-based measurements (Fig 5H) showed higher Ca^{2+} levels in IMMP1L-silenced cells.

Overall, these data reveal that the accumulation of unprocessed MICU1 by reducing IMMP1L levels mimics the effects obtained with MICU1 SD expression, thus suggesting that the impairment of MICU1 processing affects mitochondrial Ca^{2+} homeostasis.

Akt-MICU1 phosphorylation axis in ROS production and tumor development

We aimed to identify putative patho-physiological scenarios in which the MICU1 regulation by Akt could play an essential role. Glucose deprivation, a common form of metabolic stress, can induce Akt activation (Gao *et al*, 2014), and it has been recently showed that glucose withdrawal could regulate a series of molecular pathways by evoking Ca^{2+} elevations (Lee *et al*, 2018). Thus, we investigated whether the Akt-MICU1 signaling is involved in the cellular response to glucose starvation. Prolonged glucose deprivation (16 h) induced strong Akt activation, which is associated with reduced MICU1 levels (Fig EV4B). Accordingly, MICU1 appeared highly phosphorylated by Akt upon glucose starvation (Fig EV4C) and the basal mitochondrial $[Ca^{2+}]$ significantly increased, compared to cells cultured in normal conditions (Fig EV4D). Finally, the MICU1 nonphosphorylatable SA mutant showed higher stability under glucose deprivation compared to the WT form (Fig EV4E), and MICU1 SA mutant expression in *MICU1*-depleted cells restored the normal mitochondrial Ca^{2+} levels (Fig EV4F), sustaining the importance of Akt-MICU1 interplay in the glucose deprivation-mediated Ca^{2+} elevations.

Akt is overactivated in a wide range of human malignancies. Thus, we sought to determine whether mitochondrial Akt-MICU1 signaling might contribute to cancer cell proliferation and tumor growth *in vivo*. We compared the phosphorylation of MICU1 in three paired sets of tumor cell lines with and without Akt activation (Fig 6A–F and Appendix Fig S6A). The A549 lung cancer cell line displayed higher phospho-Akt levels than the mucoepidermoid carcinoma cell line H292, correlating with reduced expression of phosphatase and the tensin homolog (PTEN) (Fig 6A). An analysis of the MICU1 phosphorylation status using the PAS antibody showed more phosphorylated MICU1 in A549 cells (Fig 6B). Importantly, lower levels of both MICU1 and MICU2 proteins have been detected in Akt-positive cells (Fig 6A and Appendix Fig S6A). The PTEN-null melanoma cells (WM793b) (Paraiso *et al*, 2011) showed greater MICU1 phosphorylation levels (Fig 6C and D) and reduced amounts of MICU1 and 2 (Fig 6C and
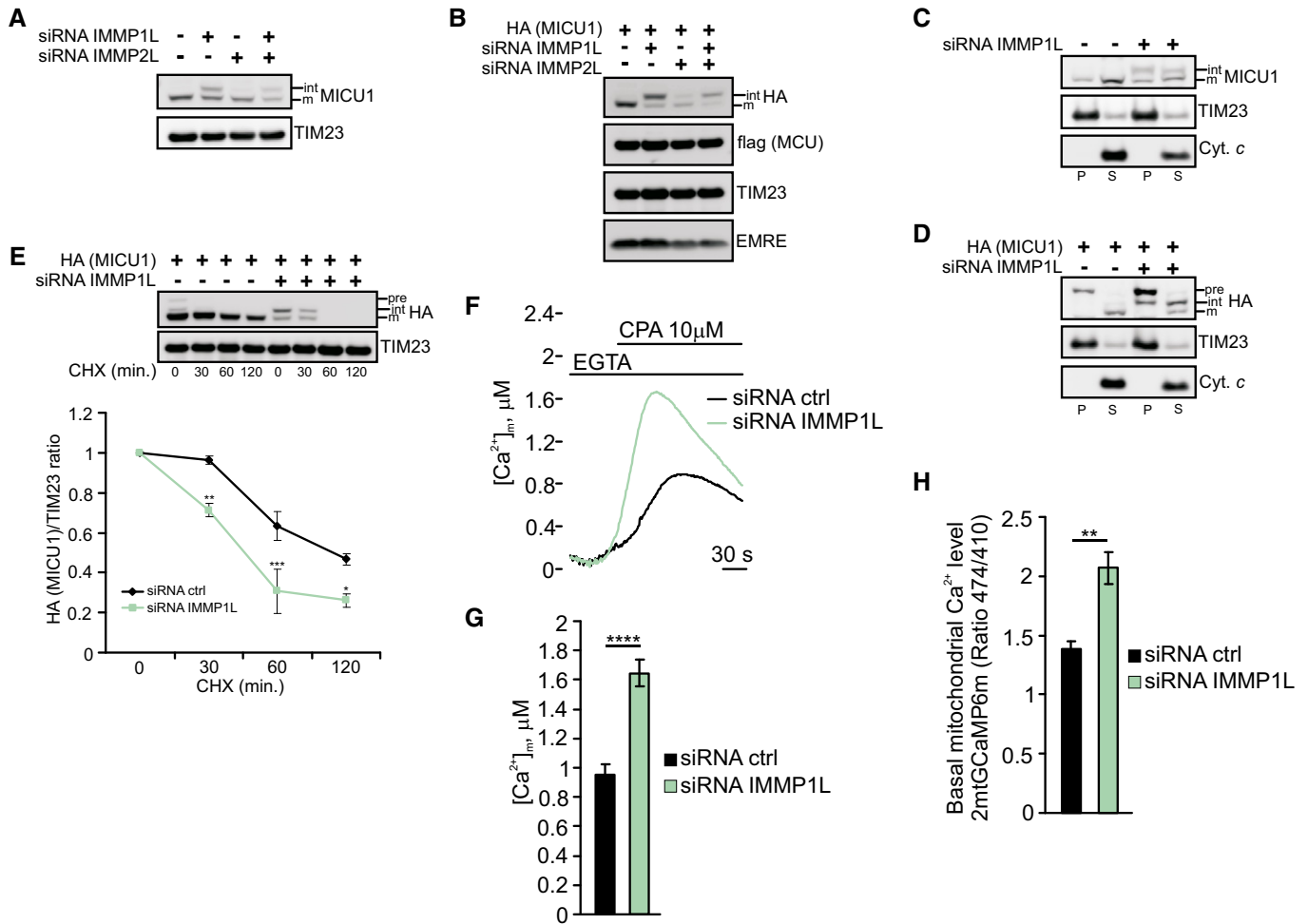
Figure 5.   IMMP1L-silencing alters MICU1 processing and basal [Ca²⁺]m levels.

A   Western blot analysis of endogenous MICU1 levels in HeLa cells upon silencing of IMMP1L and/or IMMP2L. int: intermediate; m: mature form.

B   Western blot analysis of HeLa cells transfected with the indicated constructs and silenced with IMMP1L and/or IMMP2L. int: intermediate; m: mature form. Cells were treated with 5 μM MG132 for 4 h before lysis.

C   Western blot analysis of the supernatant (S) and insoluble pellet (P) fractions of control or IMMP1L-silenced HeLa cell mitochondria following carbonate extraction at pH 10. The established integral membrane protein TIM23 and the soluble protein cytochrome c (Cyt. c) were analyzed as markers.

D   Western blot analysis of the supernatant (S) and insoluble pellet (P) fractions of control or IMMP1L-silenced HeLa cell mitochondria transfected with HA-tagged MICU1 WT following carbonate extraction at pH 10. The established integral membrane protein TIM23 and the soluble protein cytochrome c (Cyt. c) were analyzed as markers. pre: precursor; int: intermediate; m: mature form. Cells were treated with 5 μM MG132 for 4 h before lysis.

E   Control or IMMP1L-silenced HeLa cells were transfected with HA-tagged MICU1 WT. Cells were incubated with 50 μg/ml cycloheximide (CHX) for the indicated times, collected and subjected to Western blotting analysis as indicated. In the graph, the amount of HA (MICU1) is represented relative to the amount at time 0 (n = 3 independent experiments).

F, G   Representative kinetics (F) and analysis (G) of aequorin-based [Ca²⁺]m measurements in control or IMMP1L-silenced HeLa cells challenged with 10 μM cyclopiazonic acid (CPA) in the presence of 100 μM EGTA (n = 3 independent experiments).

H   Resting mitochondrial calcium levels, evaluated through ratiometric imaging of the mitochondrial-targeted GCaMP6m, in control or IMMP1L-silenced HeLa cells (n = 3 independent experiments; 37–55 cells).

Data information: (E) Means ± SD. *P < 0.05; **P < 0.01; ***P < 0.001 (one-way ANOVA); (G, H) Means ± SEM. **P < 0.01; ****P < 0.0001 (Student's t-test).
Source data are available online for this figure.

Appendix Fig S6A) than WT PTEN cells (451Lu). Similarly, the astro-cytoma cell line U87-MG, which displayed high Akt activity due to the inactivating mutations in PTEN, showed reduced expression of the MCU regulators compared with the T98G glioblastoma cells (Fig 6E and Appendix Fig S6A), which is linked to the high bulk of phospho-MICU1 (Fig 6F). These findings correlate with higher basal mitochon-drial [Ca²⁺], which was observed in both Akt-positive lung (Appendix Fig S6B and C), melanoma (Appendix Fig S6D and E), and

glioblastoma (Appendix Fig S6F and G) cancer cells. Importantly, reduction of Akt activity in Akt-positive cells (U87MG), or increasing it in Akt-negative (T98G cells), affected the levels of MICU1-2 (Appendix Fig S6H), as well as cell proliferation and colony formation (Appendix Fig S6I and J).

However, by comparing the MCF-10CA1h breast carcinoma cell line with an activating H1047R mutation in *PIK3CA* and MDA-MB231 cells lacking constitutive Akt activation (Fig EV5A) (Kadota
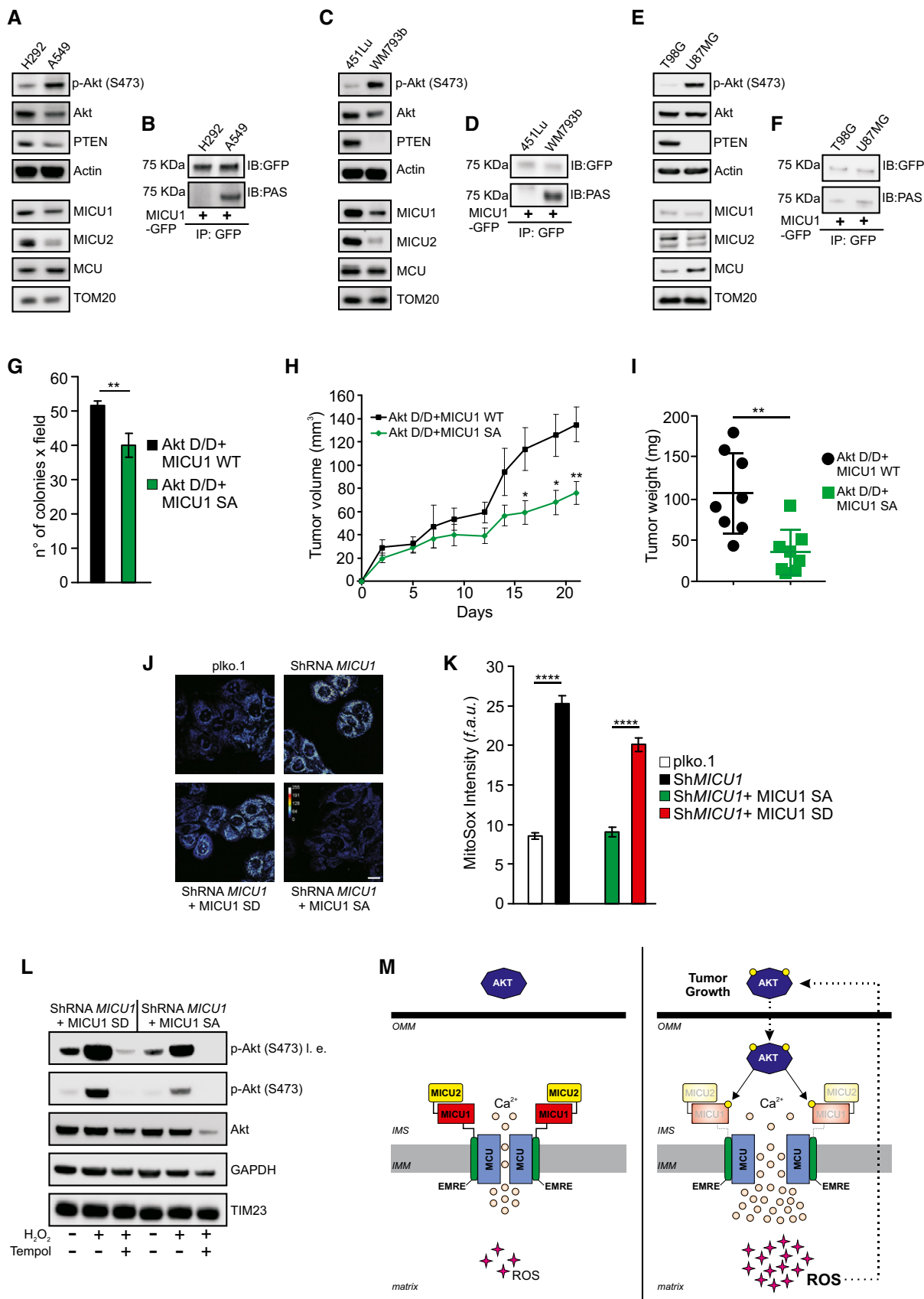
Figure 6.

◄

Figure 6. The mitochondrial Akt-MICU1 axis is critical for tumor growth.

A   Western blot analysis of MICU1 and MICU2 levels in lung cancer cells with low or high Akt activity.
B   Lung cancer cells were transfected with the GFP-tagged WT MICU1. MICU1-GFP immunocomplexes were precipitated with a GFP antibody and analyzed with a PAS (phospho-Akt substrate) antibody by Western blotting.
C   Western blot analysis of MICU1 and MICU2 levels in melanoma cells with low or high Akt activity.
D   Melanoma cells were transfected with the GFP-tagged WT MICU1. MICU1-GFP immunocomplexes were precipitated with a GFP antibody and analyzed with PAS (phospho-Akt substrate) antibody by Western blotting.
E   Western blot analysis of MICU1 and MICU2 levels in glioblastoma cells with low or high Akt activity.
F   Glioblastoma cells were transfected with the GFP-tagged WT MICU1. MICU1-GFP immunocomplexes were precipitated with GFP antibody and analyzed with PAS (phospho-Akt substrate) antibody by Western blotting.
G–I   Number of soft agar colonies (n = 3 independent experiments) (G), xenograft tumor volumes (H), and tumor weights at day 21 (n = 8 mice for each group) (I) formed by Rat2 cells stably expressing the indicated constructs.
J, K   Representative images (J) and analysis (K) of MitoSOX-based ROS measurements in ShRNA *MICU1* HeLa stable cells stably expressing either MICU1 S124D (SD) or MICU1 S124A (SA) (n = 3 independent experiments). Scale bar 10 μm. f.a.u.: fluorescence arbitrary unit.
L   ShRNA *MICU1* HeLa stable cells stably expressing either MICU1 S124D (SD) or MICU1 S124A (SA) were treated with 500 μM H_2O_2 alone or in combination with the ROS scavenger Tempol and analyzed by Western blotting as indicated. l. e.: long exposure.
M   Speculative model of the mitochondrial Akt-MICU1 axis in the regulation of tumor growth.

Data information: (G, I) Means ± SEM. **P < 0.01 (Student's t-test); (H) Means ± SEM. *P < 0.05; **P < 0.01 (multiple t-tests); (K) Means ± SEM. ****P < 0.0001 (one-way ANOVA).
Source data are available online for this figure.

$et\ al$, 2010), we detected no Akt-mediated phosphorylation of MICU1 (Fig EV5B). We reasoned that the lack of an effect of Akt on MICU1 that was observed in the MCF-10CA1h cells might be attributed to PTEN activity. A subcellular fractionation analysis revealed that MCF-10CA1h contained a discrete pool of PTEN located in mitochondria and very low levels of mitochondrial activated Akt (Fig EV5C). To further explore this process, we used *pten* gene-knockout (KO) MEFs (Fig EV5D). The PTEN KO cells expressed lower amounts of both the MICU1 and MICU2 proteins (Fig EV5E) and exhibited enhanced phosphorylation of MICU1 (Fig EV5F) compared with WT MEFs. The treatment of PTEN KO MEFs with the Akt inhibitor triciribine enhanced the stability of the MICU1-2 heterodimers (Fig EV5G). Collectively, these data indicate that in different tumor types, the activation of Akt is associated with the phosphorylation of MICU1 and a reduced MICU1-2 gatekeeping activity, supporting the notion that the N-terminal phosphorylation of MICU1 might be a key feature in human tumors bearing activated Akt. This aspect is, at least partially, dependent on the PTEN status, which might differentially affect mitochondrial Akt-MICU1 signaling based on its subcellular localization.

To examine the role of Akt-mediated MICU1 phosphorylation in Akt-driven tumor growth, we generated stable cells that overexpressed the constitutively active Akt D/D form together with either WT MICU1 or the nonphosphorylatable MICU1 S124A mutant. In an anchorage-independence growth assay, both the number and the size of the colonies formed by the Akt D/D-expressing cells were significantly reduced by the co-expression of MICU1 SA (Figs 6G and EV5H and I). Importantly, both Akt D/D-expressing cells formed palpable tumors in immunodeficient mice, but the tumor growth rate and the tumor mass weight at necropsy were reduced for the clones expressing the MICU1 SA mutant (Figs 6H and I, and EV5J). Therefore, the expression of a mutant of MICU1 that cannot be phosphorylated by Akt lowers the tumorigenic potential of transformed cells and decreases the tumor growth rate and size.

Reportedly, Akt is able to elevate the reactive oxygen species (ROS) levels in multiple cellular contexts, and this Akt-mediated ROS generation is essential for Akt-driven tumor progression (Govindarajan $et\ al$, 2007; Nogueira $et\ al$, 2008; Okoh $et\ al$, 2013). Moreover, the basal mitochondrial Ca^{2+} overload observed upon

MICU1 deficiency causes higher ROS production (Mallilankaraman $et\ al$, 2012). Thus, we investigated the possibility that MICU1 phosphorylation by Akt kinase would result in elevated mitochondrial ROS production. As expected, the Sh*MICU1* cells exhibited a higher basal level of mitochondrial ROS (Fig 6J and K). The stable introduction of the MICU1 SA mutant into MICU1-silenced cells abrogated the ROS elevation, whereas the expression of the phosphomimic MICU1 SD form failed to restore the normal ROS levels (Figs 6J and K, and EV5K). Measurements of mitochondrial hydrogen peroxide production using the ratiometric genetically encoded mitochondria–targeted HyPer probe (mito−HyPer) revealed that the MICU1 SD mutant enhanced ROS generation both in the resting condition and after the stimulation of cells with a low dose (1 μM) of H_2O_2 (Fig EV5L). Finally, glucose deprivation stimulates ROS production (Marambio $et\ al$, 2010), which is limited by expression of MICU1 SA mutant (Fig EV5M).

Exogenous H_2O_2 stimulates Akt phosphorylation, suggesting that Akt activation is redox-sensitive (Wang $et\ al$, 2000). Thus, we investigated the possibility that the increased production of ROS, which is mediated by phospho-MICU1, might affect Akt activation. Indeed, MICU1 SD-expressing cells exhibited higher levels of phosphorylated Akt than cells expressing the MICU1 SA mutant (Fig 6L). Consistently, oxidative stress strongly enhanced the Akt activation in the MICU1 SD cells, whereas application of the antioxidant compound Tempol abrogated Akt activation (Fig 6L). Altogether, we conclude that the mitochondrial Akt-mediated phosphorylation of MICU1 promotes tumor progression through deregulation of the MCU complex, thereby increasing the basal mitochondrial Ca^{2+} levels and ROS production, which, in turn, generates a positive feedback loop that sustains Akt activation (Fig 6M).

Discussion

In this study, we showed that MICU1, which is one of the pivotal regulators of the MCU channel, could be subjected to an Akt-mediated phosphorylation event that severely affects its regulatory functions on MCU. Its crucial role as a molecular gatekeeper of the uniporter complex identifies MICU1 as an attractive target

modulator of mitochondrial Ca^{2+} homeostasis. Accordingly, the protein arginine methyl transferase 1 (PRMT1) has been described to mediate the methylation of MICU1, which, in turn, desensitizes this protein to Ca^{2+} and reduces the mitochondrial Ca^{2+} uptake (Madreiter-Sokolowski *et al*, 2016). Moreover, the essential oxidoreductase Mia40/CHCHD4 can bind MICU1 and facilitate its dimerization with MICU2 (Petrungaro *et al*, 2015). Our present data underscore the importance of the N-terminal phosphorylation of the MICU1 protein in the regulation of the basal mitochondrial Ca^{2+} content. The localization of this modification is quite distant from the two EF-hand domains in the MICU1 primary sequence; thus, a mechanistic explanation of the altered functions of phospho-MICU1 could not be found in the intrinsic modification of its Ca^{2+} affinity. Our findings reveal that Akt can affect MICU1 maturation through direct phosphorylation, leading to intrinsic instability of the uniporter-associated dimer and altered mitochondrial Ca^{2+} accumulation. These data are supported by experiments in *IMMP1L*-silenced cells, which displayed higher levels of unprocessed MICU1 and increased $[Ca^{2+}]m$ contents (Fig 5). Although IMMP1-2L exists in a heterodimeric complex (Gakh *et al*, 2002), our results revealed that IMMP2L appears to play a marginal role in MICU1 processing (Fig 5A and B), suggesting that each subunit recognizes different substrates.

It is important to note that MICU1 phosphorylation appears to have an impact on abundance of both MCU and EMRE (Figs 4 and EV3), suggesting that the anomalous MICU1 processing and localization might affect the stability of other binding partners. In line with this evidence, loss of MICU1 correlates with low levels of MCU (Plovanich *et al*, 2013) and EMRE (Liu *et al*, 2016) in different cellular systems. Moreover, forced expression of MCU extended the half-life of MICU1 (Petrungaro *et al*, 2015), and a MICU1 mutant that cannot interact with MICU2 (MICU1 C463A) showed a shorter half-life, as well as a reduced expression of MCU, compared to MICU1 WT (Petrungaro *et al*, 2015). Thus, structural modifications in a single uniporter's component or the stoichiometry of MCU, EMRE, MICU1, and MICU2 influence the stability of the whole complex.

An aberrant Ca^{2+} regulation is currently thought to be a general hallmark of cancer cells, and multiple lines of evidence have noted the crucial role of Ca^{2+} homeostasis deregulation in tumor cell proliferation, apoptosis resistance, tumor development, and metastasis (Marchi & Pinton, 2016). Reduced mitochondrial Ca^{2+} uptake protects from apoptosis mediated by sustained ER Ca^{2+} release, an aspect could be especially relevant in conferring chemoresistance, or play an essential role in a specific cancer type or tumor stage. However, the correlation between high $[Ca^{2+}]m$ and ROS production is emerging as a prominent signaling route for the regulation of cancer progression (Tosatto *et al*, 2016; Ren *et al*, 2017).

MICU1 has been associated with different types of cancer, but its role remains controversial. A correlation between *MICU1* overexpression and a better prognosis has been reported in the context of mammary carcinomas, suggesting that MICU1 might function as a tumor-suppressor gene (Hall *et al*, 2014). Moreover, MICU1 appears to be a favorable prognostic marker in renal cancer (https://www. proteinatlas.org/ENSG00000107745-MICU1/pathology). In contrast, high MICU1 levels confer chemoresistance to ovarian cancer cells (Chakraborty *et al*, 2017), and *MICU1* downregulation has been associated with a higher sensitivity to apoptotic stress and impaired endothelial cell migration (Mallilankaraman *et al*, 2012). However,

an accelerated proliferation of *MICU1*-knockdown hepatocytes has been recently observed following treatment with NIM811 (Antony *et al*, 2016), which is an inhibitor of the mitochondrial permeability transition pore (mPTP), the channel responsible for the initiation of mitochondrial cell death programs (Bonora *et al*, 2015). Through inhibition of its primary target, cyclophilin D (CypD), which is a component of the mPTP, NIM811 desensitizes the mPTP to Ca^{2+}, thereby preventing cell killing (Waldmeier *et al*, 2002). Indeed, Akt activity has been widely associated with mPTP inhibition, and it was recently shown that mitochondrial Akt directly phosphorylates CypD, thereby limiting apoptosis (Ghosh *et al*, 2015). Thus, when the mPTP opening is inhibited by mitochondrial Akt or pharmacological approaches, higher mitochondrial Ca^{2+} levels might confer proliferative advantages to cancer cells without triggering apoptotic responses. Of note, our scenario agrees with recent data showing that cancer cells require basal mitochondrial Ca^{2+} uptake for survival (Cardenas *et al*, 2016).

The mitochondrial compartment has emerged as a novel critical subcellular district in which Akt exerts its kinase activity. Akt signaling regulates cellular energy metabolism and apoptosis via mechanisms that converge on mitochondria (Stiles, 2009), via its association with HK2 and VDAC (Gottlob *et al*, 2001), or via the phosphorylation of key proteins, such as BAD (Datta *et al*, 1997). In addition, Akt acts inside mitochondria, where it can phosphorylate compartment-specific substrates, including the previously cited CypD (Ghosh *et al*, 2015) and PDK1 (Chae *et al*, 2016). The intra-mitochondrial Akt activity contributes to apoptosis resistance and tumor growth and might provide a novel adaptive mechanism for tumor resistance to PI3K-based therapy (Ghosh *et al*, 2015). Our findings provide additional clues for understanding the still elusive intra-organellar activities of Akt, showing that phosphorylation of the MCU complex regulator MICU1 could sustain cancer progression by augmenting the basal mitochondrial Ca^{2+} content and ROS production (Fig 6M). Elevated levels of ROS have been detected in almost all cancers, including Akt-positive tumors (Liou & Storz, 2010). We observed reduced tumor growth with the expression of the nonphosphorylatable mutant MICU1 SA (Fig 6H), correlating with reduced mitochondrial ROS generation (Fig 6J and K), which suggests that ROS might play a pivotal role in the regulation of cell malignancy by mitochondrial Ca^{2+} accumulation. However, Ca^{2+}-related ROS generation might offer a specific therapeutic opportunity. Therefore, our data could integrate previous observations showing that cancer cells with hyperactive Akt displayed high levels of ROS and that treatment with rapamycin, which further increases Akt activation, in combination with an oxidative stress agent could be a valuable strategy for selectively eradicating Akt-positive tumor cells (Nogueira *et al*, 2008, 2018). Intriguingly, expression of a constitutively active Akt form in cells displaying very low Akt activity increased the susceptibility to glucose withdrawal-induced death (Elstrom *et al*, 2004).

We found that the bulk of PTEN located at the mitochondria might, at least partially, counteract the action of mitochondrial Akt and hence prevent MICU1 phosphorylation. This finding is consistent with the ability of mito-PTEN to inhibit Akt activation (Shen *et al*, 2015).

In conclusion, the results presented herein expand the functions of the mitochondrial pool of Akt, which are not limited to the

regulation of apoptosis and mitochondrial bioenergetics but also involve the control of mitochondrial Ca^{2+} homeostasis. Moreover, this study provides the first demonstration of the crucial role played by post-translational modifications of the MCU complex subunit MICU1 in the regulation of Akt kinase-driven tumorigenesis. Our data note the strategic importance of the association between aberrant mitochondrial Ca^{2+} levels and tumor development and highlight as alteration in the organization and activity of the MCU complex could represent critical aspects that contribute to the aggressiveness of certain cancers.

Materials and Methods

Cell cultures and transfections

HeLa, HEK293T, T98G, U87-MG (ATCC), and Rat2 (Sigma-Aldrich; passage > 70) cells, as well as PTEN WT and KO MEFs, were maintained in Dulbecco's modified Eagle's medium (DMEM), supplemented with 10% fetal bovine serum (FBS; Thermo Fisher Scientific), 2 mM L-glutamine, 100 U/ml penicillin, and 100 mg/ml streptomycin (all from Euroclone). MDA-MB-231 and H292 cells (ATCC) were maintained in RPMI supplemented with 10% FBS, L-glutamine, and penicillin/streptomycin. MCF-10CA1h cells were maintained in 1:1 DMEM:F12 supplemented with penicillin/streptomycin, 5% horse serum (Invitrogen), hEGF at 20 ng/ml (Lonza), hydrocortisone at 0.5 ng/ml (Sigma), Cholera toxin at 100 ng/ml (Sigma), insulin at 10 ng/ml (Gibco), and 10% FBS. A549 cells were maintained in F12 medium supplemented with 10% FBS, L-glutamine, penicillin/streptomycin. WM793B and 451Lu cells (Coriell) were maintained in 4:1 keratinocyte-SFM:Leibovitz L-15 (Invitrogen) supplemented with penicillin/streptomycin, insulin at 5 ng/ml, and 5% FBS.

HeLa plko and Sh*MICU1* stable clones were maintained in DMEM supplemented with 10% FBS, L-glutamine, penicillin/streptomycin, and 2 μg/ml of Puromycin.

For glucose starvation, cells were washed twice with PBS and then incubated in DMEM without glucose and pyruvate, supplemented with 10% dialyzed FBS (Thermo Fisher Scientific).

For HeLa and HEK293T cells, transient transfections were performed with a standard calcium-phosphate procedure. For the other cell lines, transient transfections were performed using JetPEI (Polyplus transfection™) or Lipofectamine 2000 (Thermo Fisher Scientific) as transfecting reagents, according to the manufacturer's instructions.

For aequorin-, GCaMP6m- and HyPer-based experiments, the cells were transiently transfected with a 3:1 cDNA ratio, where 1 is the luminescent/fluorescent indicator. The ratio of 3:1 in favor of the protein of interest versus the indicator guarantees that all the cells expressing the specific probe (and thus the only recorded by the instruments) are also expressing the protein of interest.

For TMRM-based experiments, the cells were also transfected with a 3:1 ratio, where 3 is the amount of the construct of interest and 1 is mitochondrial-targeted GFP (mt-GFP). Only cells expressing mt-GFP have been analyzed for mitochondrial membrane potential.

pcDNA3.1 (referred as "control") was used as a control for transfection unless otherwise indicated.

For silencing experiments, transfections were performed using Lipofectamine RNAiMax (Thermo Fisher Scientific) as transfecting reagents, according to the manufacturer's instructions. Akt and negative (scramble) siRNAs (final concentration 40 nM) were purchased from Cell Signaling Technology (CST). IMMP1L, IMMP2L, and negative (scramble) siRNAs (final concentration 40 nM) were purchased from Sigma-Aldrich.

Lentiviral transduction and generation of stable cell lines

Lentiviruses were produced by transfecting shRNA-targeting plasmids together with helper plasmids pCMV–VSVG and pCMV–dR8.74 into HEK293T cells. Cell supernatants were collected 48 h after transfection and were either used to infect cells or stored at −80°C. To obtain stable cell lines, cells were infected at low confluence (20%) for 24 h with lentiviral supernatants diluted 1:1 with normal culture media in the presence of 5 ng/ml of Polybrene (Sigma-Aldrich). Cells were subjected to Puromycin selection 24 h after infection.

Lentiviral ShRNAs were obtained from Sigma (MISSION ShRNA). For *MICU1* silencing, 5 shRNAs were identified and tested, TRCN0000053368 (Sh-MICU1 #1), TRCN0000053369 (Sh-MICU1 #2), TRCN0000053370 (Sh-MICU1 #3), TRCN0000053371 (Sh-MICU1 #4), and TRCN0000053372 (Sh-MICU1 #5). Among them, Sh-MICU1 #4 showed high knockdown efficiency in HeLa cells with the lowest homology with mouse sequence (NM_144822) and it was thus selected for the generation of HeLa Sh*MICU1* stable cell line.

HeLa cells stably overexpressing Sh-MICU1 #4 were transfected with both MICU1 mutant versions and selected with 500 μg/ml G418 for at least 4 weeks before assaying. The resulting Sh*MICU1* HeLa cells stably overexpressing MICU1 S124D or MICU1 S124A were maintained in complete DMEM plus 2 μg/ml of Puromycin and 500 μg/ml G418.

Gene knockout by CRISPR/Cas9

Gene knockout by CRISPR/Cas9 was performed using the published protocol (Ran *et al*, 2013). To prevent off-targets, the RNA guides (gRNA) were designed using Broad Institute's CRISPR Design tool (http://crispr.mit.edu/) uploading the sequence of the early 5′ exon of the gene of interest. Two different gRNAs targeting the 5′ of the gene were designed and used to rule out off-target effects.

The 20-nucleotide RNA guide sequence was transfected into HeLa cells with the *S. pyogenes* Cas9 (IDT) using Lipofectamine RNAiMAX Transfection Reagent (ThermoFisher). After two days of incubation, single cells were isolated by serial dilutions and expanded for 5 weeks. After one round of expansion, one clone with the lowest expression of protein was selected by Western blot and was transfected with a second round of gRNA and Cas9 protein to achieve the complete KO. Gene KO was assessed by Western blot.

Constructs and MICU1 mutants

Murine pcDNA3.1 MICU1-HA, MICU1-GFP, MICU2-flag, MCU-flag, and untagged EMRE plasmids were gently gift by Rosario Rizzuto Lab.

Creation of MICU1 mutants

The S124D and S124A mutations were introduced in the MICU1-HA and MICU1-GFP constructs by site-directed mutagenesis using the QuickChange® II Site-Directed Mutagenesis Kit (QuickChange® II XL Site-Directed Mutagenesis Kit; Agilent Technologies, Santa Clara, CA, USA), essentially as previously described (Branchini *et al*, 2013). The following forward oligonucleotides were used: 5′-GAATCCGAGCCTAC<u>GAC</u>ACACCAGACAA-3′ (S124D) and 5′-GAAT CCGAGCCTAC<u>GCG</u>ACACCAGACAA-3′ (S124A); the modified nucleotide triplets are underlined. Reverse oligonucleotides were complementary to the forward ones. All plasmids have been validated by sequencing.

Creation of pCMV5-2xMTS-HA-Akt D/D chimera

MTS (Mitochondrial Target Sequence from mouse MICU2) was amplified by PCR from MICU2 vector using the mMICU2mtsBglII-F (5′-AAAA<u>AGATCT</u>ATGGCGGCGGCTGCGGGAAG-3′) and mMICU2mtsSalI-R (5′-AAA<u>GTCGAC</u>GAGCCCGCGCCGCAGCCTTC-3′) oligonucleotides under standard conditions (restriction sites underlined). MTS was further digested with BglII and SalI restriction enzymes and then cloned into pCMV5-HA-Akt D/D, previously cut with the same enzymes, to give the pCMV5-MTS-HA-Akt D/D plasmid. In order to maintain the appropriate amino acid frame downstream of MTS in the resulting chimaeric protein, SalI site and the following triplet were removed from the pCMV5-MTS-HA-Akt D/D construct by using site-directed mutagenesis and the forward oligonucleotide 5′-CTG CGGCGCGGGCTCATGGCTTACCCATAC-3′. Reverse oligonucleotide was complementary to the forward one. MTS was then amplified again from MICU2 vector using oligonucleotides mMICU2mtsBglII-F and mMICU2mtsBglII-R (5′-AAAAGATCTGAGCCCGCGCCGCAGCCTTC-3′) under standard conditions. The resulting fragment was further digested with BglII restriction enzyme and cloned into pCMV5-MTS-HA-Akt D/D, previously cut with the same enzyme, to give the final pCMV5-2xMTS-HA-Akt D/D chimaeric construct. The same cloning procedures were applied to pCMV5-HA-Akt WT to obtain the pCMV5-2xMTS-HA-Akt WT construct.

All expression vectors have been validated by sequencing.

Immunoblot

For immunoblotting, cells were washed with ice-cold phosphate-buffered saline (PBS), scraped, and lysed, for 30 min on ice, in a buffer containing 50 mM Tris–HCl pH 7.4, 150 mM NaCl, 1% Triton X-100, 0.2% SDS, protease, and phosphates inhibitor cocktail. After centrifugation at 16,000 *g* for 10 min, proteins were quantified by the Lowry method and 10 μg of proteins, denatured for 5 min at 100°C in LDS sample buffer (Thermo Fisher Scientific) and Sample Reducing Agent (Thermo Fisher Scientific), was loaded on a Novex NuPage Bis-Tris 4–12% precast gel (Thermo Fisher Scientific). For non-denaturing conditions, the same amount of proteins were dissolved in LDS sample buffer (Thermo Fisher Scientific) and heated for 5 min at 70°C before loading. After electrophoretic separation, proteins were transferred onto PVDF membranes. To saturate unspecific binding sites, the membranes were incubated with TBS–Tween-20 (0.05%) supplemented with 5% non-fat powdered milk for 1 h at RT, and then incubated overnight with primary antibodies. The revelation was assessed by specific horseradish peroxidase-labeled secondary antibodies (Thermo Fisher Scientific),

followed by detection by chemiluminescence (Thermo Fisher Scientific), using ImageQuant LAS 4000 (GE Healthcare). Western blots shown in figures are representative of at least 3 different independent experiments.

Immunoprecipitation

For immunoprecipitation experiments, cells were seeded in 10-cm Petri dishes, transfected as indicated and lysed in an appropriate volume of lysis buffer [20 mM Tris–HCl pH 8, 137 mM NaCl, 10% Glycerol, 1% NP-40, 2 mM EDTA, protease inhibitor mixture, and Phos-STOP Phosphatase Inhibitor Cocktail (Roche Applied Science)]. The same amount of proteins from the whole-cell lysate for each condition was incubated overnight with the specific primary antibody. The immunocomplexes were captured with the appropriate protein A or protein G Sepharose (GE Healthcare). Beads were pelleted and washed three times. The bait was eluted in Laemmli sample buffer and denatured for 5 min at 100°C. The whole-cell lysate (input) and the immunoprecipitated (IP) samples were separated by SDS–PAGE, transferred to PVDF membranes, incubated with the appropriate antibodies, and developed according to standard procedures (see above).

Antibodies and reagents

Anti-HA (sc-805; sc-7392. WB 1:5,000; IF 1:200; IP 1:100), anti-HSP60 (sc-13115. WB 1:1,000; IF 1:200), anti-TOM20 (sc-17764. WB 1:5,000; IF 1:200), anti-EMRE (sc-86337. WB 1:500), were purchased from Santa Cruz Biotechnology; anti-E-cadherin (#14472. WB 1:1,000), anti-p-Akt (Ser473) (#9271. WB 1:1,000; IF 1:100), anti-Akt (#9272. WB 1:5,000), anti-p-mTOR (Ser2448) (#5536. WB 1:1,000), anti-PAS (Phospho-Akt Substrates) (#9614. WB 1:1,000; IP 1:100), anti-GAPDH (#2118. WB 1:5,000), anti-PTEN (#9559. WB 1:1,000) from Cell Signaling; anti-β-tubulin (T5201. WB 1:5,000), anti-β-actin (A1978. WB 1:10,000), anti-flag (F7425. WB 1:1,000), anti-LC3B (L7543. WB 1:1,000), anti-MICU1 (HPA037480. WB 1:1,000), anti-MCU (HPA016480. WB 1:1,000), from Sigma-Aldrich; anti-Cytochrome c (556433. WB 1:1,000), anti-TIM23 (611222. WB 1:1,000), anti-p-Ser (612546. WB 1:1,000), anti-IP3R3 (610312. WB 1:1,000; IP 1:100) from BD Transduction Laboratories; anti-MICU2 (ab1011465. WB 1:2,000), anti-AIF (ab1998. WB 1:1,000), anti-GFP (ab6556; WB 1:5,000; IP 1:100) and anti-VDAC1 (ab15895. WB 1:1,000) from Abcam; anti-GFP (No. 11814460001. WB 1:5,000; IP 1:100) from Roche. Secondary, HRP-conjugated antibodies (#31430; #31460. WB, 1:10,000) were purchased from Thermo Fisher Scientific. Secondary, AlexaFluor-conjugated antibodies (IF, 1:500) were purchased from Thermo Fisher Scientific.

2,5-di-tert-butylhydroquinone (TBHQ), Triciribine hydrate, Histamine, Cycloheximide, Cyclopiazonic Acid (CPA), MG132, and MitoTempol were purchased from Sigma-Aldrich. Rapamycin was obtained from Calbiochem and MitoSox from Thermo Fisher Scientific.

Mitochondrial membrane potential (ΔΨm) measurements

Mitochondrial ΔΨ was measured by loading cells with 20 nM tetramethyl rhodamine methyl ester (TMRM, Invitrogen) for 30 min at 37°C. Successively, cells were imaged with Nikon Swept Field

Confocal equipped with CFI Plan Apo VC60XH objective (n.a. 1.4) and an Andor DU885 EM-CCD camera, controlled by the NIS-Elements 3.2. Basal levels were normalized on fluorescence in the presence of FCCP (carbonyl cyanide p-trifluoromethoxyphenylhy-drazone, 10 μM), a strong uncoupler of oxidative phosphorylation.

Aequorin measurements

For the experiments with the chimeric aequorins targeted to the cytosol (cytAEQ) and mitochondria (mtAEQ WT and mtAEQmut), cells were seeded onto 13-mm glass coverslips and transfected as indicated. Before the measurement, cells were incubated with 5 μM coelenterazine for 1.5 h in Krebs–Ringer modified buffer (KRB; 125 mM NaCl, 5 mM KCl, 1 mM Na_3PO_4, 1 mM $MgSO_4$, 5.5 mM glucose, and 20 mM 4-(2-hydroxyethyl)-1-piperazineethanesulfonic acid [HEPES], pH 7.4, at 37°C) supplemented with 1 mM $CaCl_2$, and then transferred to the perfusion chamber. To reconstitute the chimeric aequorins targeted to the ER (erAEQmut) with high efficiency, the ER luminal $[Ca^{2+}]$ first had to be reduced, by incubation for 45 min at 4°C in KRB supplemented with 5 μM coelenterazine, 5 μM Ca^{2+} ionophore ionomycin (Sigma-Aldrich), and 600 μM EGTA. Then, cells were extensively washed with KRB supplemented with 2% bovine serum albumin and 2 mM EGTA, and then transferred to the perfusion chamber. All aequorin measurements were carried out in KRB supplemented with either 1 mM $CaCl_2$ (cytAEQ and mtAEQmut) or 100 μM EGTA (erAEQmut), and the agonist was added to the same medium as indicated in figure legends. The experiments were terminated by lysing cells with Triton X-100 in a hypotonic Ca^{2+}-rich solution (10 mM $CaCl_2$ in H_2O), thus discharging the remaining aequorin pool. The light signal was collected and calibrated into $[Ca^{2+}]$ values by an algorithm based on the Ca^{2+} response curve of aequorin at physiological conditions of pH, $[Mg^{2+}]$, and ionic strength, as previously described (Bonora *et al*, 2013).

The experiments with permeabilized cells were performed with a buffer mimicking the cytosolic ionic composition (IB): 130 mM KCl, 10 mM NaCl, 2 mM K_2HPO_4, 5 mM succinic acid, 5 mM malic acid, 1 mM $MgCl_2$, 20 mM HEPES, and 1 mM pyruvate (pH 7) at 37°C. IB was supplemented with either 100 μM EGTA (IB/EGTA) or a 2 mM EGTA-buffered $[Ca^{2+}]$ of the indicated concentration (IB/Ca^{2+}). Calculated $[Ca^{2+}]_{free}$ was predicted with CHELATOR software (Schoenmakers *et al*, 1992) and confirmed fluorimetrically with the Fura2 free acid form. Cells were permeabilized by a 1-min perfusion with 100 μM digitonin (added to IB/EGTA) during luminescence measurements. Mitochondrial Ca^{2+} uptake rate was calculated as the first derivative by using the OriginLab® software. The higher value reached during Ca^{2+} addition represents the maximal Ca^{2+} uptake rate.

Mitochondrial-targeted GCaMP6m measurements

The measurements were performed as previously described (Patron *et al*, 2014). Briefly, cells were grown on 24-mm coverslips and transfected with 2mtGCaMP6m-encoding plasmids and the indicated constructs. Imaging was performed on Cell^R multiple wavelength high-resolution fluorescence microscopy system. Cells were alternatively illuminated at 474 and 410 nm and fluorescence was collected through a 515/30-nm band-pass filter. Exposure time was set to 200 ms at 474 nm and to 400 ms at 410 nm, in order to account for the low quantum yield at the latter wavelength. At least ten fields were collected per coverslip, and each field was acquired for 30 s (1 frame/s). Analysis was performed with the Fiji open source software. Both images were background corrected frame by frame by subtracting mean pixel values of a cell-free region of interest. Data are presented as the mean of the averaged ratio of all time points.

Fura-2 AM measurements

Cytosolic free Ca^{2+} concentration ($[Ca^{2+}]c$) was evaluated using fluorescent Ca^{2+} indicator Fura-2 AM. Briefly, cells were incubated in medium supplemented with 2.5 μM Fura-2 AM for 30 min, washed with KRB to remove extracellular probe, supplied with preheated KRB (supplemented with 1 mM $CaCl_2$), and placed in a thermostated incubation chamber at 37°C on the stage of an inverted fluorescence microscope (Cell^R system). $[Ca^{2+}]c$ was calculated as previously described (Marchi *et al*, 2008).

Immunofluorescence

Cells, grown onto 13-mm coverslips and transfected as described, were washed with phosphate-buffered saline (PBS) and fixed in 4% formaldehyde for 10 min at room temperature. After washing three times with PBS, cells were permeabilized with 0.1% Triton X-100 in PBS (PBS-T) for 10 min at room temperature and then blocked with PBS-T containing 5% BSA at room temperature for 1 h. Cells were then incubated with primary antibodies overnight at 4°C, washed 3 times with PBS-T, and incubated with the appropriate isotype matched, AlexaFluor-conjugated secondary antibodies (Thermo Fisher Scientific). Coverslips were mounted with ProLong Gold Anti-fade reagent (Thermo Fisher Scientific) at room temperature, and images were acquired with confocal microscope (Zeiss LSM510) using a 63 × 1.4 NA Plan-Apochromat oil-immersion objective. Acquired images were then analyzed by using open source software Fiji.

ROS measurements

Detection of mitochondrial superoxide was performed by using MitoSOX™ Red, according to manufacturer's instructions (Molecular Probes™, Invitrogen). Briefly, cells grown to 50–80% confluence on glass coverslips were incubated with 5 μM MitoSOX in Hank's Buffered Salt Solution containing calcium and magnesium (HBSS), for 15 min at 37°C in a CO_2 incubator and then washed three times with HBSS. Microscopy imaging was performed on the confocal microscope Zeiss LSM510, using a 63 × 1.4 NA Plan-Apochromat oil-immersion objective, 514 nm excitation laser, and a 580 ± 30 nm fluorescence detection range. Alternatively, Mito-SOX™ Red fluorescence intensity were also measured using Tali® Image-based Cytometer (Molecular Probes™, Invitrogen).

For mitochondrial hydrogen peroxide level measurements, cells were cultured on 24-mm glass coverslips and transfected with the ratiometric fluorescent probe with mitochondrial localization pHyPer-dMito (mt-HyPer) (Marchi *et al*, 2015). After 24 h of expression, cells were maintained in Krebs–Ringer buffer (KRB) supplemented with 1 mM $CaCl_2$, and placed in an open Leyden chamber

on a 37°C thermostated stage. The experiments were performed on Cell^R Olympus multiple wavelength high-resolution epi-fluorescence microscope. 494/406-nm excitation filters and a 500-nm long-pass beam splitter were used, and an image pair was obtained in every 200 ms with a 40× objective. The fluorescence data collected were expressed as emission ratios.

Real-time PCR

Total RNA was extracted with TRIzol® Reagent (Invitrogen), RNAs were purified by using RNeasy Mini Kit (Qiagen), and DNase digestion was performed with RNase-Free DNase Set (Qiagen). The RNA quality and concentration were measured using the NanoDropTM ND-1000 (Thermo Fisher Scientific). For the first-strand cDNA synthesis, 1,000 ng of total RNA of each sample was reverse-transcribed with M-MLV Reverse Transcriptase (Invitrogen), following the manufacturer's protocol. Human primers were selected for each target gene with Primer 3 software. Real-time PCRs were carried out using the designed primers at a concentration of 300 nM and FastStart SYBR Green Master (Roche Diagnostics) on a Rotor-Gene 3000 (Corbett Research). Thermal cycling conditions were as follows: 10-min denaturation at 95°C, followed by 40 cycles of denaturation for 10 s at 95°C; annealing for 20 s at 60°C; and elongation for 30 s at 72°C. Values were normalized to the expression of the glyceraldehyde-3-phosphate dehydrogenase (GAPDH), whose abundance did not change under our experimental conditions.

Mitochondria isolation and topology analysis

Both crude and pure mitochondria fractions from cells and mouse livers were prepared as previously described (Wieckowski *et al*, 2009).

For the localization study, 100 µg of crude mitochondria isolated from Hek293T was resuspended in a mitochondrial buffer containing 0.5 mM EGTA-Tris and 10 mM Tris-MOPS (pH 7.4), with (intact mitochondria) or without (to induce OMM rupture) 250 mM sucrose, or with 1% Triton X-100 for inducing IMM rupture. All conditions were treated with 100 µg/ml Proteinase K (PK) for 30′ at 4°C, and then, 5 mM PMSF was added to stop the digestion. Mitochondrial proteins were precipitated following the TCA/Acetone method, and 5 µg of each fractions was used for Western blot analysis.

For the alkaline carbonate extraction study, 200 µg of crude mitochondria was pelleted and resuspended in 400 µl of 100 mM Na_2CO_3 buffer adjusted to different pHs (ranging from 7.4 to 12.5). After incubation on ice for 30 min, samples were centrifuged at 100,000 *g* for 30 min at 4°C. Mitochondrial proteins were precipitated following the TCA/Acetone method.

Soft agar colony formation assay

Assays were performed in triplicate in 6-well plates. Base agar consisted of 0.5% agar (Sigma-Aldrich), 1× DMEM, 500 µg/ml G418, and 10% FBS. Top agar consisted of 0.3% agar, 1× DMEM, 500 µg/ml G418, and 10% FBS with $2.5 × 10^4$ Rat2 cells per well. Cells were incubated in 5% CO_2 at 37°C for 4 weeks and then stained with 0.005% crystal violet. To quantify the colonies, five randomly selected images of each replicate were captured using a

Leica DM IL LED microscope with a 4× magnification. Colonies were counted automatically using a custom made macro in the Fiji software. Briefly, dark objects were thresholded using the Yen algorithm and counted through the analyze particles tool.

Tumor xenograft studies

To measure tumor formation by Rat2 fibroblasts stably expressing a constitutively active Akt form together with MICU1 WT or MICU1 S124A mutant, 6-week-old NOD SCID® mice (Charles River) were shaved on the right flank one day prior to injection and injected subcutaneously with $1 × 10^7$ tumor cells in 200 µl of PBS. 8–9 mice per cell line were injected. Tumor growth was monitored by daily measurements of tumor length (L) and width (W), and tumor volume was estimated using the formula: tumor volume = $\frac{1}{2}(L × W^2)$. After 21 days, mice were sacrificed and the tumors were dissected and weighed.

Statistical analysis

Quantitative data are presented as means ± SEM if not indicated otherwise. Statistical analyses were performed using an unpaired two-tailed *t*-test (two groups) or one-way ANOVA with Tukey's correction (for groups of three or more). For grouped analyses, two-way ANOVA with correction for multiple comparisons using the Holm–Sidak method was performed. Normal distribution of data was assessed by applying a D'Agostino & Pearson omnibus normality test. *F*-test was used to compare variances between groups. A *P*-value < 0.05 was considered significant.

other experiments. SMa, CG, MPi, LG, GK, and PP interpreted the data. SMa, GK, and PP wrote the manuscript.

Conflict of interest

References

Antony AN, Paillard M, Moffat C, Juskeviciute E, Correnti J, Bolon B, Rubin E, Csordas G, Seifert EL, Hoek JB, Hajnoczky G (2016) MICU1 regulation of mitochondrial Ca(2+) uptake dictates survival and tissue regeneration. *Nat Commun* 7: 10955

Barksdale KA, Bijur GN (2009) The basal flux of Akt in the mitochondria is mediated by heat shock protein 90. *J Neurochem* 108: 1289−1299

Baughman JM, Perocchi F, Girgis HS, Plovanich M, Belcher-Timme CA, Sancak Y, Bao XR, Strittmatter L, Goldberger O, Bogorad RL, Koteliansky V, Mootha VK (2011) Integrative genomics identifies MCU as an essential component of the mitochondrial calcium uniporter. *Nature* 476: 341−345

Bonora M, Giorgi C, Bononi A, Marchi S, Patergnani S, Rimessi A, Rizzuto R, Pinton P (2013) Subcellular calcium measurements in mammalian cells using jellyfish photoprotein aequorin-based probes. *Nat Protoc* 8: 2105−2118

Bonora M, Wieckowsk MR, Chinopoulos C, Kepp O, Kroemer G, Galluzzi L, Pinton P (2015) Molecular mechanisms of cell death: central implication of ATP synthase in mitochondrial permeability transition. *Oncogene* 34: 1608

Boroughs LK, DeBerardinis RJ (2015) Metabolic pathways promoting cancer cell survival and growth. *Nat Cell Biol* 17: 351−359

Branchini A, Campioni M, Mazzucconi MG, Biondo F, Mari R, Bicocchi MP, Bernardi F, Pinotti M (2013) Replacement of the Y450 (c234) phenyl ring in the carboxyl-terminal region of coagulation factor IX causes pleiotropic effects on secretion and enzyme activity. *FEBS Lett* 587: 3249−3253

Cardenas C, Muller M, McNeal A, Lovy A, Jana F, Bustos G, Urra F, Smith N, Molgo J, Diehl JA, Ridky TW, Foskett JK (2016) Selective vulnerability of cancer cells by inhibition of Ca(2+) transfer from endoplasmic reticulum to mitochondria. *Cell Rep* 14: 2313−2324

Chae YC, Vaira V, Caino MC, Tang HY, Seo JH, Kossenkov AV, Ottobrini L, Martelli C, Lucignani G, Bertolini I, Locatelli M, Bryant KG, Ghosh JC, Lisanti S, Ku B, Bosari S, Languino LR, Speicher DW, Altieri DC (2016) Mitochondrial Akt regulation of hypoxic tumor reprogramming. *Cancer Cell* 30: 257−272

Chakraborty PK, Mustafi SB, Xiong X, Dwivedi SKD, Nesin V, Saha S, Zhang M, Dhanasekaran D, Jayaraman M, Mannel R, Moore K, McMeekin S, Yang D, Zuna R, Ding K, Tsiokas L, Bhattacharya R, Mukherjee P (2017) MICU1 drives glycolysis and chemoresistance in ovarian cancer. *Nat Commun* 8: 14634

Csordas G, Golenar T, Seifert EL, Kamer KJ, Sancak Y, Perocchi F, Moffat C, Weaver D, de la Fuente Perez S, Bogorad R, Koteliansky V, Adijanto J, Mootha VK, Hajnoczky G (2013) MICU1 controls both the threshold and cooperative activation of the mitochondrial Ca(2)(+) uniporter. *Cell Metab* 17: 976−987

Danese A, Patergnani S, Bonora M, Wieckowski MR, Previati M, Giorgi C, Pinton P (2017) Calcium regulates cell death in cancer: roles of the mitochondria and mitochondria-associated membranes (MAMs). *Biochim Biophys Acta* 1858: 615−627

Datta SR, Dudek H, Tao X, Masters S, Fu H, Gotoh Y, Greenberg ME (1997) Akt phosphorylation of BAD couples survival signals to the cell-intrinsic death machinery. *Cell* 91: 231−241

De Stefani D, Raffaello A, Teardo E, Szabo I, Rizzuto R (2011) A forty-kilodalton protein of the inner membrane is the mitochondrial calcium uniporter. *Nature* 476: 336−340

Dufner A, Andjelkovic M, Burgering BM, Hemmings BA, Thomas G (1999) Protein kinase B localization and activation differentially affect S6 kinase 1 activity and eukaryotic translation initiation factor 4E-binding protein 1 phosphorylation. *Mol Cell Biol* 19: 4525−4534

Elstrom RL, Bauer DE, Buzzai M, Karnauskas R, Harris MH, Plas DR, Zhuang H, Cinalli RM, Alavi A, Rudin CM, Thompson CB (2004) Akt stimulates aerobic glycolysis in cancer cells. *Cancer Res* 64: 3892−3899

Frezza C (2014) The role of mitochondria in the oncogenic signal transduction. *Int J Biochem Cell Biol* 48: 11−17

Gakh O, Cavadini P, Isaya G (2002) Mitochondrial processing peptidases. *Biochim Biophys Acta* 1592: 63−77

Galluzzi L, Kepp O, Kroemer G (2012) Mitochondria: master regulators of danger signalling. *Nat Rev Mol Cell Biol* 13: 780−788

Gao M, Liang J, Lu Y, Guo H, German P, Bai S, Jonasch E, Yang X, Mills GB, Ding Z (2014) Site-specific activation of AKT protects cells from death induced by glucose deprivation. *Oncogene* 33: 745−755

Gaude E, Frezza C (2014) Defects in mitochondrial metabolism and cancer. *Cancer Metab* 2: 10

Ghosh JC, Siegelin MD, Vaira V, Faversani A, Tavecchio M, Chae YC, Lisanti S, Rampini P, Giroda M, Caino MC, Seo JH, Kossenkov AV, Michalek RD, Schultz DC, Bosari S, Languino LR, Altieri DC (2015) Adaptive mitochondrial reprogramming and resistance to PI3K therapy. *J Natl Cancer Inst* 107: dju502

Giorgi C, Marchi S, Pinton P (2018) The machineries, regulation and cellular functions of mitochondrial calcium. *Nat Rev Mol Cell Biol* 19: 713−730

Gottlieb E, Tomlinson IP (2005) Mitochondrial tumour suppressors: a genetic and biochemical update. *Nat Rev Cancer* 5: 857−866

Gottlob K, Majewski N, Kennedy S, Kandel E, Robey RB, Hay N (2001) Inhibition of early apoptotic events by Akt/PKB is dependent on the first committed step of glycolysis and mitochondrial hexokinase. *Genes Dev* 15: 1406−1418

Govindarajan B, Sligh JE, Vincent BJ, Li M, Canter JA, Nickoloff BJ, Rodenburg RJ, Smeitink JA, Oberley L, Zhang Y, Slingerland J, Arnold RS, Lambeth JD, Cohen C, Hilenski L, Griendling K, Martinez-Diez M, Cuezva JM, Arbiser JL (2007) Overexpression of Akt converts radial growth melanoma to vertical growth melanoma. *J Clin Invest* 117: 719−729

Hall DD, Wu Y, Domann FE, Spitz DR, Anderson ME (2014) Mitochondrial calcium uniporter activity is dispensable for MDA-MB-231 breast carcinoma cell survival. *PLoS ONE* 9: e96866

Hanahan D, Weinberg RA (2011) Hallmarks of cancer: the next generation. *Cell* 144: 646−674

Herrmann JM, Hell K (2005) Chopped, trapped or tacked−protein translocation into the IMS of mitochondria. *Trends Biochem Sci* 30: 205−211

Hill JM, De Stefani D, Jones AW, Ruiz A, Rizzuto R, Szabadkai G (2014) Measuring baseline Ca(2+) levels in subcellular compartments using genetically engineered fluorescent indicators. *Methods Enzymol* 543: 47−72

Kadota M, Yang HH, Gomez B, Sato M, Clifford RJ, Meerzaman D, Dunn BK, Wakefield LM, Lee MP (2010) Delineating genetic alterations for tumor progression in the MCF10A series of breast cancer cell lines. *PLoS ONE* 5: e9201

Khan MT, Wagner L II, Yule DI, Bhanumathy C, Joseph SK (2006) Akt kinase phosphorylation of inositol 1,4,5-trisphosphate receptors. *J Biol Chem* 281: 3731−3737

Lee HY, Itahana Y, Schuechner S, Fukuda M, Je HS, Ogris E, Virshup DM, Itahana K (2018) Ca(2+)-dependent demethylation of phosphatase PP2Ac

promotes glucose deprivation-induced cell death independently of inhibiting glycolysis. *Sci Signal* 11: eaam7893

Liou GY, Storz P (2010) Reactive oxygen species in cancer. *Free Radic Res* 44: 479 – 496

Littlepage LE, Adler AS, Kouros-Mehr H, Huang G, Chou J, Krig SR, Griffith OL, Korkola JE, Qu K, Lawson DA, Xue Q, Sternlicht MD, Dijkgraaf GJ, Yaswen P, Rugo HS, Sweeney CA, Collins CC, Gray JW, Chang HY, Werb Z (2012) The transcription factor ZNF217 is a prognostic biomarker and therapeutic target during breast cancer progression. *Cancer Discov* 2: 638 – 651

Liu JC, Liu J, Holmstrom KM, Menazza S, Parks RJ, Fergusson MM, Yu ZX, Springer DA, Halsey C, Liu C, Murphy E, Finkel T (2016) MICU1 serves as a molecular gatekeeper to prevent *in vivo* mitochondrial calcium overload. *Cell Rep* 16: 1561 – 1573

Logan CV, Szabadkai G, Sharpe JA, Parry DA, Torelli S, Childs AM, Kriek M, Phadke R, Johnson CA, Roberts NY, Bonthron DT, Pysden KA, Whyte T, Munteanu I, Foley AR, Wheway G, Szymanska K, Natarajan S, Abdelhamed ZA, Morgan JE *et al* (2014) Loss-of-function mutations in MICU1 cause a brain and muscle disorder linked to primary alterations in mitochondrial calcium signaling. *Nat Genet* 46: 188 – 193

Madreiter-Sokolowski CT, Klec C, Parichatikanond W, Stryeck S, Gottschalk B, Pulido S, Rost R, Eroglu E, Hofmann NA, Bondarenko AI, Madl T, Waldeck-Weiermair M, Malli R, Graier WF (2016) PRMT1-mediated methylation of MICU1 determines the UCP2/3 dependency of mitochondrial Ca(2+) uptake in immortalized cells. *Nat Commun* 7: 12897

Mallilankaraman K, Doonan P, Cardenas C, Chandramoorthy HC, Muller M, Miller R, Hoffman NE, Gandhirajan RK, Molgo J, Birnbaum MJ, Rothberg BS, Mak DO, Foskett JK, Madesh M (2012) MICU1 is an essential gatekeeper for MCU-mediated mitochondrial Ca(2+) uptake that regulates cell survival. *Cell* 151: 630 – 644

Manning BD, Cantley LC (2007) AKT/PKB signaling: navigating downstream. *Cell* 129: 1261 – 1274

Marambio P, Toro B, Sanhueza C, Troncoso R, Parra V, Verdejo H, Garcia L, Quiroga C, Munafo D, Diaz-Elizondo J, Bravo R, Gonzalez MJ, Diaz-Araya G, Pedrozo Z, Chiong M, Colombo MI, Lavandero S (2010) Glucose deprivation causes oxidative stress and stimulates aggresome formation and autophagy in cultured cardiac myocytes. *Biochim Biophys Acta* 1802: 509 – 518

Marchi S, Rimessi A, Giorgi C, Baldini C, Ferroni L, Rizzuto R, Pinton P (2008) Akt kinase reducing endoplasmic reticulum Ca^{2+} release protects cells from Ca^{2+} -dependent apoptotic stimuli. *Biochem Biophys Res Commun* 375: 501 – 505

Marchi S, Marinello M, Bononi A, Bonora M, Giorgi C, Rimessi A, Pinton P (2012) Selective modulation of subtype III IP(3)R by Akt regulates ER Ca(2)(+) release and apoptosis. *Cell Death Dis* 3: e304

Marchi S, Lupini L, Patergnani S, Rimessi A, Missiroli S, Bonora M, Bononi A, Corra F, Giorgi C, De Marchi E, Poletti F, Gafa R, Lanza G, Negrini M, Rizzuto R, Pinton P (2013) Downregulation of the mitochondrial calcium uniporter by cancer-related miR-25. *Curr Biol* 23: 58 – 63

Marchi S, Corricelli M, Trapani E, Bravi L, Pittaro A, Delle Monache S, Ferroni L, Patergnani S, Missiroli S, Goitre L, Trabalzini L, Rimessi A, Giorgi C, Zavan B, Cassoni P, Dejana E, Retta SF, Pinton P (2015) Defective autophagy is a key feature of cerebral cavernous malformations. *EMBO Mol Med* 7: 1403 – 1417

Marchi S, Pinton P (2016) Alterations of calcium homeostasis in cancer cells. *Curr Opin Pharmacol* 29: 1 – 6

Nogueira V, Park Y, Chen CC, Xu PZ, Chen ML, Tonic I, Unterman T, Hay N (2008) Akt determines replicative senescence and oxidative or oncogenic premature senescence and sensitizes cells to oxidative apoptosis. *Cancer Cell* 14: 458 – 470

Nogueira V, Patra KC, Hay N (2018) Selective eradication of cancer displaying hyperactive Akt by exploiting the metabolic consequences of Akt activation. *Elife* 7: e32213

Okoh VO, Felty Q, Parkash J, Poppiti R, Roy D (2013) Reactive oxygen species via redox signaling to PI3K/AKT pathway contribute to the malignant growth of 4-hydroxy estradiol-transformed mammary epithelial cells. *PLoS ONE* 8: e54206

Paillard M, Csordas G, Szanda G, Golenar T, Debattisti V, Bartok A, Wang N, Moffat C, Seifert EL, Spat A, Hajnoczky G (2017) Tissue-specific mitochondrial decoding of cytoplasmic Ca(2+) signals is controlled by the stoichiometry of MICU1/2 and MCU. *Cell Rep* 18: 2291 – 2300

Paraiso KH, Xiang Y, Rebecca VW, Abel EV, Chen YA, Munko AC, Wood E, Fedorenko IV, Sondak VK, Anderson AR, Ribas A, Palma MD, Nathanson KL, Koomen JM, Messina JL, Smalley KS (2011) PTEN loss confers BRAF inhibitor resistance to melanoma cells through the suppression of BIM expression. *Cancer Res* 71: 2750 – 2760

Patron M, Checchetto V, Raffaello A, Teardo E, Vecellio Reane D, Mantoan M, Granatiero V, Szabo I, De Stefani D, Rizzuto R (2014) MICU1 and MICU2 finely tune the mitochondrial Ca2 + uniporter by exerting opposite effects on MCU activity. *Mol Cell* 53: 726 – 737

Perocchi F, Gohil VM, Girgis HS, Bao XR, McCombs JE, Palmer AE, Mootha VK (2010) MICU1 encodes a mitochondrial EF hand protein required for Ca (2+) uptake. *Nature* 467: 291 – 296

Petrungaro C, Zimmermann KM, Kuttner V, Fischer M, Dengjel J, Bogeski I, Riemer J (2015) The Ca(2+)-dependent release of the Mia40-induced MICU1-MICU2 Dimer from MCU regulates mitochondrial Ca(2+) uptake. *Cell Metab* 22: 721 – 733

Plovanich M, Bogorad RL, Sancak Y, Kamer KJ, Strittmatter L, Li AA, Girgis HS, Kuchimanchi S, De Groot J, Speciner L, Taneja N, Oshea J, Koteliansky V, Mootha VK (2013) MICU2, a paralog of MICU1, resides within the mitochondrial uniporter complex to regulate calcium handling. *PLoS ONE* 8: e55785

Prevarskaya N, Skryma R, Shuba Y (2011) Calcium in tumour metastasis: new roles for known actors. *Nat Rev Cancer* 11: 609 – 618

Quiros PM, Langer T, Lopez-Otin C (2015) New roles for mitochondrial proteases in health, ageing and disease. *Nat Rev Mol Cell Biol* 16: 345 – 359

Raffaello A, De Stefani D, Sabbadin D, Teardo E, Merli G, Picard A, Checchetto V, Moro S, Szabo I, Rizzuto R (2013) The mitochondrial calcium uniporter is a multimer that can include a dominant-negative pore-forming subunit. *EMBO J* 32: 2362 – 2376

Ran FA, Hsu PD, Wright J, Agarwala V, Scott DA, Zhang F (2013) Genome engineering using the CRISPR-Cas9 system. *Nat Protoc* 8: 2281 – 2308

Ren T, Zhang H, Wang J, Zhu J, Jin M, Wu Y, Guo X, Ji L, Huang Q, Yang H, Xing J (2017) MCU-dependent mitochondrial Ca(2+) inhibits NAD(+)/SIRT3/SOD2 pathway to promote ROS production and metastasis of HCC cells. *Oncogene* 36: 5897 – 5909

Sancak Y, Markhard AL, Kitami T, Kovacs-Bogdan E, Kamer KJ, Udeshi ND, Carr SA, Chaudhuri D, Clapham DE, Li AA, Calvo SE, Goldberger O, Mootha VK (2013) EMRE is an essential component of the mitochondrial calcium uniporter complex. *Science* 342: 1379 – 1382

Schoenmakers TJ, Visser GJ, Flik G, Theuvenet AP (1992) CHELATOR: an improved method for computing metal ion concentrations in physiological solutions. *Biotechniques* 12: 870 – 874, 876-9

Shen SM, Guo M, Xiong Z, Yu Y, Zhao XY, Zhang FF, Chen GQ (2015) AIF inhibits tumor metastasis by protecting PTEN from oxidation. *EMBO Rep* 16: 1563 – 1580

Stiles BL (2009) PI-3-K and AKT: onto the mitochondria. *Adv Drug Deliv Rev* 61: 1276 – 1282

Szado T, Vanderheyden V, Parys JB, De Smedt H, Rietdorf K, Kotelevets L, Chastre E, Khan F, Landegren U, Soderberg O, Bootman MD, Roderick HL (2008) Phosphorylation of inositol 1,4,5-trisphosphate receptors by protein kinase B/Akt inhibits Ca^{2+} release and apoptosis. *Proc Natl Acad Sci USA* 105: 2427−2432

Tosatto A, Sommaggio R, Kummerow C, Bentham RB, Blacker TS, Berecz T, Duchen MR, Rosato A, Bogeski I, Szabadkai G, Rizzuto R, Mammucari C (2016) The mitochondrial calcium uniporter regulates breast cancer progression via HIF-1alpha. *EMBO Mol Med* 8: 569−585

Tsai MF, Phillips CB, Ranaghan M, Tsai CW, Wu Y, Willliams C, Miller C (2016) Dual functions of a small regulatory subunit in the mitochondrial calcium uniporter complex. *Elife* 5: e15545

Vogtle FN, Wortelkamp S, Zahedi RP, Becker D, Leidhold C, Gevaert K, Kellermann J, Voos W, Sickmann A, Pfanner N, Meisinger C (2009) Global analysis of the mitochondrial N-proteome identifies a processing peptidase critical for protein stability. *Cell* 139: 428−439

Vogtle FN, Prinz C, Kellermann J, Lottspeich F, Pfanner N, Meisinger C (2011) Mitochondrial protein turnover: role of the precursor intermediate peptidase Oct1 in protein stabilization. *Mol Biol Cell* 22: 2135−2143

Waldeck-Weiermair M, Malli R, Parichatikanond W, Gottschalk B, Madreiter-Sokolowski CT, Klec C, Rost R, Graier WF (2015) Rearrangement of MICU1 multimers for activation of MCU is solely controlled by cytosolic Ca(2+). *Sci Rep* 5: 15602

Waldmeier PC, Feldtrauer JJ, Qian T, Lemasters JJ (2002) Inhibition of the mitochondrial permeability transition by the nonimmunosuppressive cyclosporin derivative NIM811. *Mol Pharmacol* 62: 22−29

Wang X, McCullough KD, Franke TF, Holbrook NJ (2000) Epidermal growth factor receptor-dependent Akt activation by oxidative stress enhances cell survival. *J Biol Chem* 275: 14624−14631

Wieckowski MR, Giorgi C, Lebiedzinska M, Duszynski J, Pinton P (2009) Isolation of mitochondria-associated membranes and mitochondria from animal tissues and cells. *Nat Protoc* 4: 1582−1590

Yang L, Dan HC, Sun M, Liu Q, Sun XM, Feldman RI, Hamilton AD, Polokoff M, Nicosia SV, Herlyn M, Sebti SM, Cheng JQ (2004) Akt/protein kinase B signaling inhibitor-2, a selective small molecule inhibitor of Akt signaling with antitumor activity in cancer cells overexpressing Akt. *Cancer Res* 64: 4394−4399